On the Development of Near-Ground Rotation During Tornadogenesis

Robert Peter Davies-Jones [a]

[a] *Remote corner of a black hole*

D-J Research Papers, **4**.

June 2025

Corresponding author: bobdj1066@yahoo.com

ABSTRACT

Although isolated supercells rotate aloft soon after storm initiation, they take considerable time to develop significant vertical vorticity near the ground and thereafter a tornado. Without frictional interaction with the ground, only a quasi-tornado forms. In theory, its vertical vorticity can be maintained by abrupt upward tilting of almost streamwise horizontal vorticity in its corner region. This inviscid steady "in-and-up" mechanism only requires surface inflow and vortex suction. There is no inward advection of circulation, which must occur in a tornado to compensate for diffusive circulation losses.

Observations and numerical simulations find that parcels that enter a tornado have previously descended. These parcels have cyclonic vorticity at the nadir of their trajectories and anticyclonic vorticity further upstream. The trajectory of a parcel that entered a tornado in an axisymmetric model was found. The parcel's barotropic vorticity in the tornado is due to tilting and stretching of the almost streamwise vorticity that it has at the time when it has no vertical vorticity. The parcel reaches its nadir slightly later when its vertical vorticity is cyclonic but small compared to its horizontal vorticity there. The parcel's vertical velocity and vertical vorticity do not vanish simultaneously.

The slight departures from totally streamwise vorticity are consequential. Theory and a simulation show that, at each low level, growth of circulation of the tornado's narrowing parent updraft necessitates cyclonic vorticity at the updraft edge and associated inward transport of circulation. Without this transport, the updraft's circulation decays via diffusive losses to the downdraft and ground.

KEYWORDS: Tornadoes; Tornadogenesis; Supercells; Vorticity

SIGNIFICANCE STATEMENT

How tornadoes form is still unsettled. It is agreed that rotation develops aloft in supercell storms through tilting of environmental streamwise vorticity. Prior to producing tornadoes, the storm must generate near-ground rotation. Simulations indicate that parcels entering an intensifying cyclonic tornado have descended and that, at the lowest points (nadirs) of their trajectories, these parcels have developed slight cyclonic vorticity even though they had anticyclonic vorticity further upstream. The cyclonic vorticity that a parcel possesses in the

tornado is due to tilting and stretching of the large, almost streamwise, vorticity that it had at its nadir. Slight cyclonic vorticity at the nadir is found herein to be significant because the updraft's rotation at low heights could never develop without it.

1. Introduction

In supercells there is little vertical vorticity near the ground initially. How rotation first develops near the ground and how tornadoes form thereafter is still a matter of debate (Fischer et al. 2024).

In simulations of supercells, a small-scale resolved vortex that does not break the thermodynamic speed limit (Fiedler 1994) is referred to here as a quasi-tornado (QT) and one that does is called a tornado. This distinction between QT and tornado is important. When a no-slip lower boundary condition (LBC) is imposed on the vortex's tangential velocity, the vortex loses circulation to the ground and an unbalanced inward pressure-gradient force drives inflow along the ground to very near the axis where it erupts upward in an axial jet. Despite the circulation loss, the vortex spins up into a tornado with winds more than three times the speed limit. When the LBC is free slip, the prognostic equation that determines eddy viscosity has a zero solution (Davies-Jones 2021), which allows for an unchanging environment. Inside the storm, the turbulence parameterization stays inactive (Markowski and Bryan 2016) and the computed eddy viscosity remains zero or nearly so. Because friction is unimportant in the free-slip case, there is a cyclostrophic barrier that prevents inflowing parcels from getting beside the axis, the speed limit is not exceeded, and the vortex is a QT. Simulations with semi-slip LBCs quantified with a drag coefficient are less problematic, but random eddies have to be introduced to stir the flow. Otherwise, the turbulence is confined to a thin layer next to the ground, resulting in excessive vertical shear there (Markowski and Bryan 2016) that could lead to premature tornado formation (Davies-Jones 2021) and improbable vortex structure.

In their analysis of a QT in a 3D supercell simulation with a free-slip lower boundary condition and no explicit diffusion (Markowski and Richardson 2014). Rotunno et al. (2017) assumed a steady frictionless quasi-Beltrami flow in the vicinity of the tornado. They showed that there is negligible vertical vorticity at the nadir (lowest point) of the streamlines in the vicinity of a steady inviscid QT. They concluded that "cyclonic vorticity at the nadirs

77 is helpful but not necessary for rapid near-surface amplification of vertical vorticity since
78 vertical vorticity in the vortex originates from abrupt upward turning of near-ground
79 horizontal streamwise vorticity". Because the flow is steady, this "in-and-up" mechanism
80 assumes an already developed QT. It does not apply to a tornado where there is significant
81 loss of circulation to the ground and outward diffusion of circulation from the core. At each
82 height, the rotation of a tornado's parent updraft has to be maintained by an inflow with
83 cyclonic vorticity at the updraft edge whereas that of a steady inviscid QT does not.

84 Davies-Jones (1982) had argued earlier that, during tornadogenesis, cyclonic vorticity had
85 to develop in a downdraft. Tilting of near-ground horizontal vorticity by an updraft would
86 produce vertical vorticity only in air that is rising away from the ground. This would not
87 apply if streamlines turned abruptly upward at the ground, but this situation would require the
88 pressure deficit of an already developed vortex (Davies-Jones at al. 2001, p. 180).

89 Davies-Jones and Brooks (1993, hereafter DJB) were interested in how circulation near
90 the ground first develops. The DJB or "downdraft" mechanism states that buoyancy causes
91 the vortex lines to separate from the streamlines if they were coincident initially and thus to
92 produce Lamb vector (the cross product of velocity and vorticity) if there were none initially.
93 In hindsight, buoyancy is relevant only to the extent that it produces Lamb vector.
94 Regardless of its origins, the Lamb vector is the fundamental quantity. As observed in their
95 simulation, and in many subsequent ones, the DJB mechanism produces vertical vorticity at
96 the nadir of parcel trajectories. DJB speculated that vertical stretching of this vertical
97 vorticity at the nadir could be responsible for the development of near-ground rotation.
98 However, Rotunno et al. (2017) showed that upward tilting of the nadiral streamwise
99 vorticity is a much larger source of near-ground rotation. This paper finds the real reason
100 why cyclonic vorticity at the nadir is important in tornadogenesis.

101 Davies-Jones (2008, hereafter DJ08) built a simple axisymmetric model that adequately
102 demonstrated tornadogenesis while avoiding some of the difficulties that more sophisticated
103 3D supercell simulations have with initiation, turbulence parameterization and lower
104 boundary conditions. Although unrealistic, assumptions of axisymmetry and constant eddy
105 viscosity simplify computations and facilitate physical interpretation. Use of a
106 streamfunction assures mass conservation. Staggered grids are problematic because some
107 variables are undefined at the ground and axis. Therefore, the DJ08 model uses an
108 unstaggered grid. The uniform mesh is square so that the vortex boundary layer and core are

resolved equally. The Reynolds number is low enough, 2000, for the over-thick boundary layer to be adequately resolved. Initiation from a state far from equilibrium or any realistic situation is not used so there is no 'early, unphysical tornado phase' (Fischer and Dahl 2022). Instead, the initial state is a balanced Beltrami state (one without Lamb vector) that resembles a midlevel mesocyclone without significant rotation near the ground as the ascent of air and upward tilting of horizontal vorticity are gradual. When hydrometeors are introduced gradually through the top of the domain, hydrometeor drag upsets the balance. Downward and inward transport of angular momentum (AM) in the DJ08 model ultimately results in a tornado. The vortex that forms in this model breaks the thermodynamic speed limit by a factor greater than three so it is a tornado, not a QT.

Based mainly on results from 3D supercell simulations, Boyer et al. (2020), Fischer and Dahl (2022) and Fischer et al. (2024) suggest that, in simulations devoid of initial vertical vorticity, the initial emergence of vertical vorticity near the ground is due to the DJB mechanism, but, once a mature QT or tornado develops, the vertical vorticity in the vortex originates totally from upward tilting and subsequent stretching of horizontal vorticity in the corner region of the vortex (the "in-and-up mechanism"). Their hypothesis is based largely on a synthesis of steady inviscid flow theory or on simulations with free-slip or semi-slip LBCs (without artificial introduction of vertical vorticity). [Note that in simulations with semi-slip LBCs, random eddies have to be introduced to stir the flow in order to prevent excessive vertical shear next to the ground (Markowski and Bryan 2016)]. Their theory presupposes that there is a steady inviscid solution that resembles a tornado. If there is such a solution, it is probably a Beltrami flow. Is there a tornado-like Beltrami flow?

The purpose of this paper is to revise the DJB mechanism. In other words, to show, via theory and a simple numerical simulation (from DJ08), how near-ground rotation develops when there is none initially and no vorticity is added artificially. The analysis uses circulation analysis around moving horizontal circuits (Davies-Jones 2004, hereafter DJ04; Davies-Jones and Markowski 2021). The circulation around a horizontal circuit is equal to the mean vertical vorticity in the plane area enclosed by the curve. Via Stokes' theorem, it also equals the line integral of the wind tangent to the closed curve (or for axisymmetric flow 2π times the AM). Understanding tornadogenesis is the motivation so the circuit is chosen to be the edge at a low fixed height of a tornado-producing updraft and its rate of change of

circulation is the main interest. At each height, parcel properties and horizontal forces at the updraft edge determine changes in updraft circulation.

2. Analysis

The analysis considers the rate of change of circulation around a variable, horizontal, low-height curve $L(t)$ at height h that encloses a horizontally moving horizontal area $A(t)$. In general, the points on $L(t)$ are neither fixed nor constrained to move with the flow.

The equation of motion for supercell flow in a non-rotating reference frame is

$$\frac{\partial \mathbf{v}}{\partial t} + \left(\mathbf{v_H} \cdot \nabla_H + w\frac{\partial}{\partial z}\right)\mathbf{v} = -\alpha\nabla p - g\mathbf{k} - gq_l\mathbf{k} + \mathbf{F}, \tag{2.1}$$

where t is time, $\mathbf{k}$ is the unit upward vector, subscript H denotes horizontal, $\mathbf{v} \equiv \mathbf{v}_H + w\mathbf{k}$ is the wind vector, p is pressure, α is specific volume, g is gravitational acceleration, q_l is the hydrometeor mixing ratio, and $\mathbf{F} \equiv \mathbf{F}_H + \mathbf{F}\bullet\mathbf{k}\,\mathbf{k}$ is friction. For simplicity, we assume the incompressible continuity equation,

$$\boldsymbol{\nabla} \cdot \mathbf{v} = 0. \tag{2.2}$$

The vorticity vector is $\boldsymbol{\omega} \equiv \nabla\times\mathbf{v} \equiv \boldsymbol{\omega}_H + \zeta\mathbf{k}$. Taking $\mathbf{k}\bullet\nabla\times$ of (2.1) and using (2.2) and vector identities (including $\nabla\bullet\boldsymbol{\omega} = 0$) yields the vertical-vorticity equation,

$$\begin{aligned}\frac{\partial \zeta}{\partial t} &= \boldsymbol{\omega} \cdot \boldsymbol{\nabla} w - \mathbf{v} \cdot \boldsymbol{\nabla}\zeta + \mathbf{k} \cdot (-\nabla\alpha \times \nabla p + \nabla \times \mathbf{F}) \\ &= \boldsymbol{\nabla} \cdot (w\boldsymbol{\omega} - \zeta\mathbf{v}) + \mathbf{k} \cdot \nabla \times (-\alpha\nabla_H p + \mathbf{F}_H) \\ &= \boldsymbol{\nabla_H} \cdot (w\boldsymbol{\omega}_H - \zeta\mathbf{v}_H) + \mathbf{k} \cdot \nabla \times (-\alpha\nabla_H p + \mathbf{F}_H).\end{aligned} \tag{2.3}$$

The circulation Γ around $L(t)$ is

$$\Gamma = \oint_{L(t)} \mathbf{v}_H \cdot d\mathbf{x} = \iint_{A(t)} \zeta dA \tag{2.4}$$

where $d\mathbf{x}$ is a counterclockwise directed vector element of arclength around $L(t)$. Let $A(t)$ be comprised of points $\mathbf{x}(t)$ that move horizontally with velocity $\mathbf{V}_H[\mathbf{x}(t), t]$. The rate of change of circulation around $L(t)$ is

$$\frac{\delta\Gamma}{\delta t} = \iint_{A(t)} \frac{\delta\zeta}{\delta t} dA + \iint_{A(t)} \zeta \frac{\delta}{\delta t}(dA)\,. \tag{2.5}$$

where $\delta/\delta t$ at a point denotes rate of change following the moving point. The rate of change of ζ following a point of $A(t)$ is

$$\frac{\delta\zeta}{\delta t} = \frac{\partial\zeta}{\partial t} + \mathbf{V}_H \cdot \nabla_H \zeta \tag{2.6}$$

(Petterssen 1956, p. 48) and the rate of change of a moving areal element is

$$\frac{\delta}{\delta t}(dA) = (\nabla_H \cdot \mathbf{V}_H) dA. \tag{2.7}$$

Therefore,

$$\frac{\delta\Gamma}{\delta t} = \iint_{A(t)} \left(\frac{\partial\zeta}{\partial t} + \mathbf{V}_H \cdot \nabla_H \zeta\right) dA + \iint_{A(t)} \zeta \nabla_H \cdot \mathbf{V}_H dA$$

$$= \iint_{A(t)} \left[\frac{\partial\zeta}{\partial t} + \nabla_H \cdot (\zeta \mathbf{V}_H)\right] dA. \tag{2.8}$$

Introducing (2.3) into (2.8) and using Stokes' theorem and the 2D version of Gauss' divergence theorem yields

$$\frac{\delta\Gamma}{\delta t} = \iint_{A(t)} [\nabla_H \cdot (w\boldsymbol{\omega}_H - \zeta \mathbf{v}_H + \zeta \mathbf{V}_H) + \mathbf{k} \cdot \nabla \times (-\alpha \nabla_H p + \mathbf{F}_H)] dA$$

$$= \oint_{L(t)} (w\boldsymbol{\omega}_H - \zeta \mathbf{v}_H + \zeta \mathbf{V}_H) \cdot \mathbf{n} ds - \oint_{L(t)} \alpha \nabla_H p \cdot d\mathbf{x} + \oint_{L(t)} \mathbf{F}_H \cdot d\mathbf{x}. \tag{2.9}$$

Here **n** is the unit *outward horizontal* normal to $L(t)$ and ds denotes a scalar element of arclength. The vectors **n**, **t**, and **k** form a right-handed set of orthonormal basis functions where **t** = **k**×**n** is the unit counterclockwise tangent vector to $L(t)$. The circulation around $L(t)$, and hence the mean vertical vorticity within $L(t)$, is determined solely by the values on the curve of the curve-relative wind, the vorticity, and the horizontal force. The terms on the right of (2.9) are, respectively, the rates of change of barotropic (denoted by subscript BT), baroclinic (BC), and frictional (F) circulation.

We may rewrite the barotropic term in (2.9) as

$$\frac{\delta\Gamma_{\mathrm{BT}}}{\delta t} = \oint_{L(t)} \zeta(\mathbf{v}_H - \mathbf{V}_H) \cdot (-\mathbf{n}) ds - \oint_{L(t)} w\boldsymbol{\omega}_H \cdot (-\mathbf{n}) ds. \tag{2.10}$$

The barotropic circulation around the moving horizontal boundary increases due to (i) correlation of vertical vorticity and inflow at the boundary and (ii) downward turning of

187 *inward directed horizontal vorticity at the boundary*. When $L(t)$ is the updraft edge (locus of
188 $w = 0$), there is no tilting of horizontal vorticity at the curve, and the barotropic circulation
189 grows only when overall the curve-relative inflow has cyclonic vorticity and any relative
190 outflow has anticyclonic vorticity. When $L(t)$ is the locus of $\zeta = 0$ and the horizontal vorticity
191 is inward, the vertical velocity has to be negative on average for the barotropic circulation to
192 increase. The barotropic circulation around $L(t)$ is steady if w and ζ both vanish on $L(t)$.

193 Via vector identities,

194 $$(\mathbf{v} - \mathbf{V}_H) \times \boldsymbol{\omega} \cdot \mathbf{t} = (\mathbf{v} - \mathbf{V}_H) \times \boldsymbol{\omega} \cdot (\mathbf{k} \times \mathbf{n})$$
$$= (\mathbf{v} - \mathbf{V}_H) \cdot \mathbf{k}(\boldsymbol{\omega} \cdot \mathbf{n}) - (\mathbf{v} - \mathbf{V}_H) \cdot \mathbf{n}(\boldsymbol{\omega} \cdot \mathbf{k}) = (w\boldsymbol{\omega}_H - \zeta\mathbf{v} + \zeta\mathbf{V}_H) \cdot \mathbf{n}, \qquad (2.11)$$

195 so an alternative version of (2.10) is

196 $$\frac{\delta \Gamma_{\mathrm{BT}}}{\delta t} = \oint_{L(t)} (\mathbf{v} - \mathbf{V}_H) \times \boldsymbol{\omega} \cdot \mathbf{t} ds \qquad (2.12)$$

197 where the right side is the circulation around $L(t)$ of the curve-relative Lamb vector,
198 $(\mathbf{v}–\mathbf{V}_H)\times\boldsymbol{\omega}$ and $\mathbf{t}ds = d\mathbf{x}$. C*irculation of the curve-relative Lamb vector equals the rate of*
199 *change of the barotropic circulation*. The **t**-component of the curve-relative Lamb vector is
200 positive at a curve point when the projection of the $\mathbf{v}–\mathbf{V}_H$ vector onto the plane containing **n**
201 and **k** is left of the projected vorticity vector when viewed in the direction of increasing **t**
202 (Fig. 1). At all curve points where the curve-relative Lamb vector is positive, the vorticity
203 can have an upward component and $\mathbf{v}–\mathbf{V}_H$ a downward component as shown in Fig. 1. At the
204 nadir of a trajectory (where $w = 0$), the integrand in (2.12) is positive only if the vertical
205 vorticity is positive there.

206

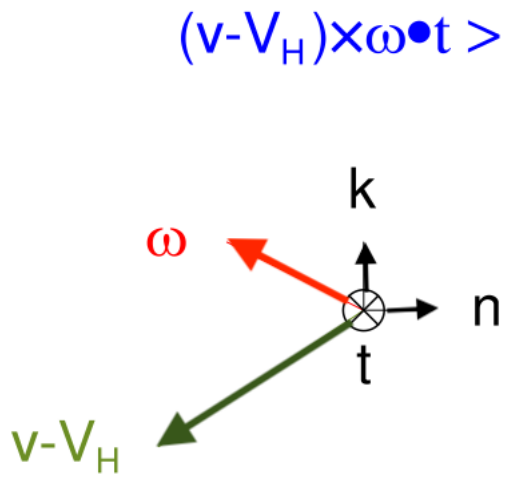

Fig. 1. The relationship between curve-relative wind and vorticity vectors and positive curve-relative Lamb vector at a point on the horizontal circuit $L(t)$. The unit vectors **n** and **k** are in the plane of the diagram with **k** upward and **n** outward normal to $L(t)$. The unit vector **t** is into the page. It is the counterclockwise tangent to the curve. The red and green arrows depict the projections of the vorticity and curve-relative wind vectors onto the plane containing **n** and **k**. The **t**-components of these vectors do not contribute to Lamb vector circulation. When the vorticity is inclined upward relative to the curve-relative wind vector, the **t**-component of the Lamb vector is positive.

Let $L(t)$ is the well-defined perimeter at height h of an updraft surrounded by a compensating or another type of downdraft. To satisfy $\delta w/\delta t = 0$, an isopleth of w at a point Q moves normal to itself with the velocity

$$\mathbf{V}_H \cdot \mathbf{n}]_{\mathrm{Q}} = -\frac{\partial w/\partial t}{\partial w/\partial n}\Bigg]_{\mathrm{Q}} \tag{2.13}$$

(Stewart 1945, p. 420). By introducing the vertical component of (2.1) into (2.11) and using $w = 0$ at Q, we obtain

$$(\mathbf{V}_H - \mathbf{v}_H)\cdot \mathbf{n}]_{\mathrm{Q}} = -\frac{G}{\partial w/\partial n}\Bigg]_{\mathrm{Q}} \tag{2.14}$$

where G is the net vertical force per unit mass [the vertical component of the right side of (2.1)]. The left side is the inflow into the updraft at Q. On the right, $\partial w/\partial n$ is negative by definition. Thus, there is inflow into the updraft at Q when the vertical force is positive there. Introducing (2.14) and (2.10) into (2.9) gives

$$\left.\frac{\delta\Gamma}{\delta t}\right]_{w=0} = -\oint_{L(t)} \zeta \frac{G}{\partial w/\partial n}\, ds - \oint_{L(t)} \alpha dp + \oint_{L(t)} \mathbf{F}_H \cdot \mathbf{t} ds\,. \tag{2.15}$$

after again using $w = 0$ on $L(t)$. On the right of (2.15), the second term represent rate of change of baroclinic circulation around the level curve. It is zero around a coaxial circle in axisymmetric flow or, more generally, when α is horizontally constant. The third term is the rate of change of frictional circulation. Because friction near the ground slows flow, it opposes circulation growth. Thus, *the barotropic circulation around an updraft increases when cyclonic vorticity and upward force are correlated at its edge* (see also Davies-Jones, 1984 eq. 37; DJ04 eq.4.7; Davies-Jones and Markowski, 2021 eq. 7). Rotunno and Klemp (1982) showed that updrafts propagate towards the side of the storm where the vertical force is upward and away from the side where it is negative. Therefore, the barotropic circulation around the updraft edge of a right-moving supercell increases when the updraft moves towards the cyclonic side and away from the anticyclonic side (DJ04), and is steady when the vertical vorticity vanishes at the updraft edge.

For brevity, henceforth we describe only the situation for a cyclonically rotating updraft in the northern-hemisphere. Then, the circulation Γ is positive and increases as the updraft rotates faster. Consider five cases.

a. Beltrami flow

The first one is when the flow is a viscous incompressible Beltrami one (Shapiro 1993). In a incompressible Beltrami flow (BF), $\boldsymbol{\omega} = \lambda \mathbf{v}$ where λ is a constant and $\mathbf{V}_H = 0$ because the contours don't move. The modified Lamb vector vanishes in (2.11) and hence the barotropic term in (2.9) is zero. The baroclinic term is zero because α is constant. Since $\mathbf{F}_H = -\nu_e \lambda^2 \mathbf{v}_H$ (where ν_e is a constant eddy viscosity), the friction equals $-\nu_e \lambda^2 \Gamma$. By solving (2.9) in this case, we find that Γ decays at the rate $-\nu_e \lambda^2 t$ in a BF.

b. Steady, inviscid, final approach

The second case is the final approach of a parcel near the ground into a QT analyzed by Rotunno et al. (2017). They characterized the final-approach flow as steady, barotropic, and inviscid, and concluded that "vertical vorticity at a parcel's nadir, although helpful, does not need to be positive for rapid near- surface amplification of the parcel's vertical vorticity". Since the flow is steady and inviscid, $\mathbf{V}_H = \mathbf{F}_H = 0$. Setting $\zeta = 0$ at the updraft edge in (2.9)

then yields $\delta\Gamma/\delta t|_{w=0} = 0$ so the circulation around the updraft is constant. As demonstrated later in this section, a parcel can acquire vertical vorticity in the updraft through tilting if it has horizontal vorticity at its nadir. Hence, their statement is correct.

c. Tornadogenesis in real fluid

The third case pertains to the generation of low-level updraft rotation during tornadogenesis. The friction term in (2.15) acts to reduce Γ as in a Beltrami flow (see above) and also during tornadogenesis where friction reduces centrifugal force in a tornado's boundary layer so that parcels driven by unbalanced inward pressure-gradient force can reach closer to the axis and exceed the thermodynamic speed limit (Fiedler and Rotunno 1986; Fiedler 1994). Therefore, the first term in (2.15) must be the one responsible for increasing circulation around the low-level updraft and it must be large enough to overcome the rate at which Γ is lost through by friction. Since tornadoes occur in very convergent flow, we assume that the relative flow is into the updraft (as in section 2b). As shown above, this requires, at the updraft edge, upward force and positive ζ. The original version of the DJB mechanism specified that cyclonic vorticity at the nadir arises from baroclinicity, but it can also be due to other causes such as frictional torque or presence in the initial state. If we fleetingly choose $L(t)$ to be a different closed curve, one along which $\zeta = 0$, then we conclude from (2.9) that the circulation about this curve increases if $w < 0$ on it since the horizontal vorticity is inward in the boundary layer of a cyclonic vortex. Hence, the vertical vorticity switches from negative to positive in the downdraft that surrounds the tornado's parent updraft.

Fischer et al. (2024) infer from the above conclusion of Rotunno et al/ (2017) that "the transition to the in-and-up mechanism marks an important change in the dynamics because, for the tornado to persist, parcels entering the tornado now do not need to arrive with vertical vorticity, i.e., the downdraft mechanism is not necessary anymore. Only horizontal vorticity is required, which is typically large in the tornado boundary layer because of surface drag acting on the tornadic winds". However, from (2.9) for steady flow, parcels that enter a steady cyclonic tornado must have small positive ζ at their nadirs because, in order for the total circulation around the parent updraft to be constant, the barotropic circulation must be positive to compensate for the circulation lost through frictional interaction with the ground and through outward diffusion. When friction is included, the downdraft mechanism applies to steady tornadoes in addition to intensifying ones. The in-and-up scenario may still occur

when the total circulation is declining rather than steady. But Fischer et al.'s (2024) further statement that "Embedded in the supercell mesocyclone and updraft, the tornado then can theoretically persist unchanged, constantly generating and tilting its own vorticity" is inexact.

d. Circular circuit

For the fourth case, we choose as our horizontal curve a circle $C(t)$ of radius $r_0(t)$ and area $A(t)$. We introduce local cylindrical coordinates (r, ϕ, z) with origin O at the center of the circle. In these coordinates, the wind, the velocity of the curve points, and vorticity are $\mathbf{v} \equiv (u, v, w)$, $\mathbf{V}_H \equiv (U, 0, 0)$, and

$$\boldsymbol{\omega} \equiv (\xi, \eta, \zeta) = \left(\frac{1}{r}\frac{\partial w}{\partial \phi} - \frac{1}{r}\frac{\partial M}{\partial z}, \frac{\partial u}{\partial z} - \frac{\partial w}{\partial r}, \frac{1}{r}\frac{\partial M}{\partial r} - \frac{1}{r}\frac{\partial u}{\partial \phi}\right) \tag{2.16}$$

where $M \equiv vr$ is the AM about the center O. On the circle,

$$\mathbf{n}ds = r_0 d\phi \hat{\mathbf{r}}, \qquad d\mathbf{x} = \mathbf{t}ds = r_0 d\phi \widehat{\boldsymbol{\phi}} \tag{2.17}$$

where $\hat{\mathbf{r}}\ (= \mathbf{n})$ and $\widehat{\boldsymbol{\phi}}\ (= \mathbf{t})$ are the radial and azimuthal unit vectors, and

$$(w\boldsymbol{\omega} - \zeta \mathbf{v}_H + \zeta \mathbf{V}_H) \cdot \mathbf{n} = w\left(\frac{1}{r_0}\frac{\partial w}{\partial \phi} - \frac{1}{r_0}\frac{\partial M}{\partial z}\right) - (u - U)\left(\frac{1}{r_0}\frac{\partial M}{\partial r} - \frac{1}{r_0}\frac{\partial u}{\partial \phi}\right). \tag{2.18}$$

Introducing (2.17) and (2.18) into (2.9) produces

$$\frac{\delta \Gamma}{\delta t} = -\oint_{C(t)} \left[(u - U)\frac{\partial M}{\partial r} + w\frac{\partial M}{\partial z}\right] d\phi - \oint_{C(t)} \alpha \frac{\partial p}{\partial \phi} d\phi + \oint_{C(t)} r_0 \mathbf{F} \cdot \widehat{\boldsymbol{\phi}} d\phi\,. \tag{2.19}$$

Thus, the rate of change of barotropic circulation around a level circle C(t) is equal to the line integral around C(t) of AM advection.

e. Axisymmetric flow

The fifth case assumes axisymmetric flow. It is relevant because the example in section 3 is for axisymmetric flow, because asymmetric swirling flows become nearly axisymmetric as a vortex is approached (Shtern et al. 1997), and because axisymmetry is frequently invoked in tornado theory (Rotunno and Bluestein 2024). The horizontal closed curve is now a circle with center at the axis of symmetry. Applying (2.14) to an axisymmetric central updraft with inflow ($u < 0$) tells us that *the updraft will contract* ($U < 0$) when *the sum of the advection of vertical velocity and the upward force at the edge is negative*.

For axisymmetric flow, we obtain

315 $$\frac{1}{2\pi}\frac{\delta\Gamma}{\delta t}=\frac{\delta M}{\delta t}=-(\mathbf{v}-\mathbf{V}_H)\cdot\nabla M+r_0\mathbf{F}\cdot\widehat{\boldsymbol{\phi}}. \quad (2.20)$$

316 by performing the integration in (2.19). *Following a circle point in axisymmetric flow, the*
317 *rate of change of AM equals advection of AM plus the frictional torque*, which near the
318 ground acts to decrease AM. The relationship between advection of AM [the first term on
319 the right of (2.20)] and the circulation of the curve-relative Lamb vector is apparent in this
320 case from

321 $$-\left[(u-U)\frac{\partial M}{\partial r}+w\frac{\partial M}{\partial z}\right]=r_0w\xi-r_0(u-U)\zeta=r_0(\mathbf{v}-\mathbf{V}_H)\times\boldsymbol{\omega}\cdot\widehat{\boldsymbol{\phi}}. \quad (2.21)$$

322 [via (2.16) for axisymmetric flow]. When $w = 0$ on $C(t)$ and there is flow into the updraft
323 ($u–U < 0$), we see from (2.21) that *growth of the updraft's barotropic circulation requires*
324 *cyclonic vorticity at the edge of the updraft*.

325 The vertical vorticity of a parcel in the tornado is due to tilting of its nadiral streamwise
326 vorticity and to vertical stretching of its nadiral vertical vorticity. We can show this for
327 unsteady, barotropic, axisymmetric flow as follows. The continuity equation for
328 incompressible, axisymmetric flow is

329 $$\frac{\partial u}{\partial r}+\frac{u}{r}+\frac{\partial w}{\partial z}=0. \quad (2.22)$$

330 Lagrangian dynamics reveals the variation of vorticity along trajectories. Let (r_i, z_i) denote
331 the initial position of a parcel that is currently at (r, z). The Lagrangian continuity equation
332 for axisymmetric incompressible flow is

333 $$\frac{r}{r_i}\frac{\partial(r,z)}{\partial(r_i,z_i)}=1 \quad (2.23)$$

334 where

335 $$\frac{\partial(r,z)}{\partial(r_i,z_i)}\equiv\frac{\partial r}{\partial r_i}\frac{\partial z}{\partial z_i}-\frac{\partial r}{\partial z_i}\frac{\partial z}{\partial r_i} \quad (2.24)$$

336 is a Jacobian. We verify (2.23) by taking the material derivative of both sides of (2.23), and
337 then introducing (2.23) and using Jacobian properties (Margenau and Murphy, 1956, pp. 18-
338 19). This procedure recovers the Eulerian continuity equation (2.22) from the Lagrangian
339 continuity equation as done by Salmon (1998, p.6) for Cartesian instead of cylindrical
340 coordinates. By conservation of AM in inviscid flow,

$$M(r,z) = M(r_i, z_i). \tag{2.25}$$

From (2.16) for axisymmetric flow, the chain rule, (2.23), and Jacobian properties,

$$\zeta = \frac{1}{r}\frac{\partial M}{\partial r} = \frac{1}{r}\frac{\partial(M,z)}{\partial(r,z)}\frac{r}{r_i}\frac{\partial(r,z)}{\partial(r_i,z_i)} = \frac{1}{r_i}\frac{\partial(M,z)}{\partial(r_i,z_i)}$$

$$= \frac{1}{r_i}\frac{\partial M}{\partial r_i}\frac{\partial z}{\partial z_i} - \frac{1}{r_i}\frac{\partial M}{\partial z_i}\frac{\partial z}{\partial r_i} = \frac{\partial z}{\partial r_i}\xi_i + \frac{\partial z}{\partial z_i}\zeta_i \tag{2.26}$$

where ξ_i and ζ_i are the parcel's initial radial and vertical vorticity. Similarly,

$$\xi = \frac{\partial r}{\partial r_i}\xi_i + \frac{\partial r}{\partial z_i}\zeta_i. \tag{2.27}$$

In matrix form,

$$\begin{bmatrix}\xi \\ \zeta\end{bmatrix} = \begin{bmatrix}\partial r/\partial r_i & \partial r/\partial z_i \\ \partial z/\partial r_i & \partial z/\partial z_i\end{bmatrix}\begin{bmatrix}\xi_i \\ \zeta_i\end{bmatrix}. \tag{2.28}$$

Let the initial position (r_i, z_i) be at the nadir of a trajectory. *The parcel's barotropic vorticity depends on its vorticity at its nadir and its deformation from the nadiral time to the current time*. In (2.26), the second term on the right is due to vertical stretching in convergent flow of the initial vertical vorticity. The first term is due to upward tilting and stretching in convergent flow of the initial horizontal vorticity. In the idealized case of a steady inviscid vortex, $\zeta_i = 0$ at the nadir and the vertical vorticity in the vortex is due entirely to the first term on the right of (2.26) as found by Rotunno et al. (2017) and Boyer and Dahl (2020). In the model simulation presented in the next section, the second term is nonzero but negligible.

3. Example

The main simulation of the axisymmetric DJ08 model, described briefly in section 1 and exhaustively in Davies-Jones (2025), provides an example. The flow is nondimensionalized by the height H of the domain and the initial maximum updraft velocity W_0. To roughly scale the flow to a supercell, we assume H = 12000 m and W_0 = 33.3 m s^{-1}. One unit of time, H/W_0, is then 360 s. The boundary conditions are no slip on the azimuthal velocity and free slip otherwise so that features of a turbulent vortex boundary layer are crudely replicated in the axisymmetric model with constant eddy viscosity (Lewellen 1993, p. 24). The initial state of this model is a Beltrami flow ($\boldsymbol{\omega} = \lambda \mathbf{v}$) that resembles a midlevel mesocyclone (Figs.

2 and 3). The initial updraft radius is 0.442. At the start, winds near the ground-axis intersection are light. In axisymmetric flow, AM advection, $-\mathbf{v}\bullet\nabla M$, equals $r\xi w - r\zeta u$ by (2.16), and hence is zero initially (Fig. 3). AM advection is initiated by release of hydrometeors. While the updraft is contracting at low heights, a tornado forms at t =5.4 as AM increases locally in the corner region of the domain. It reaches maximum intensity at t = 6.1.

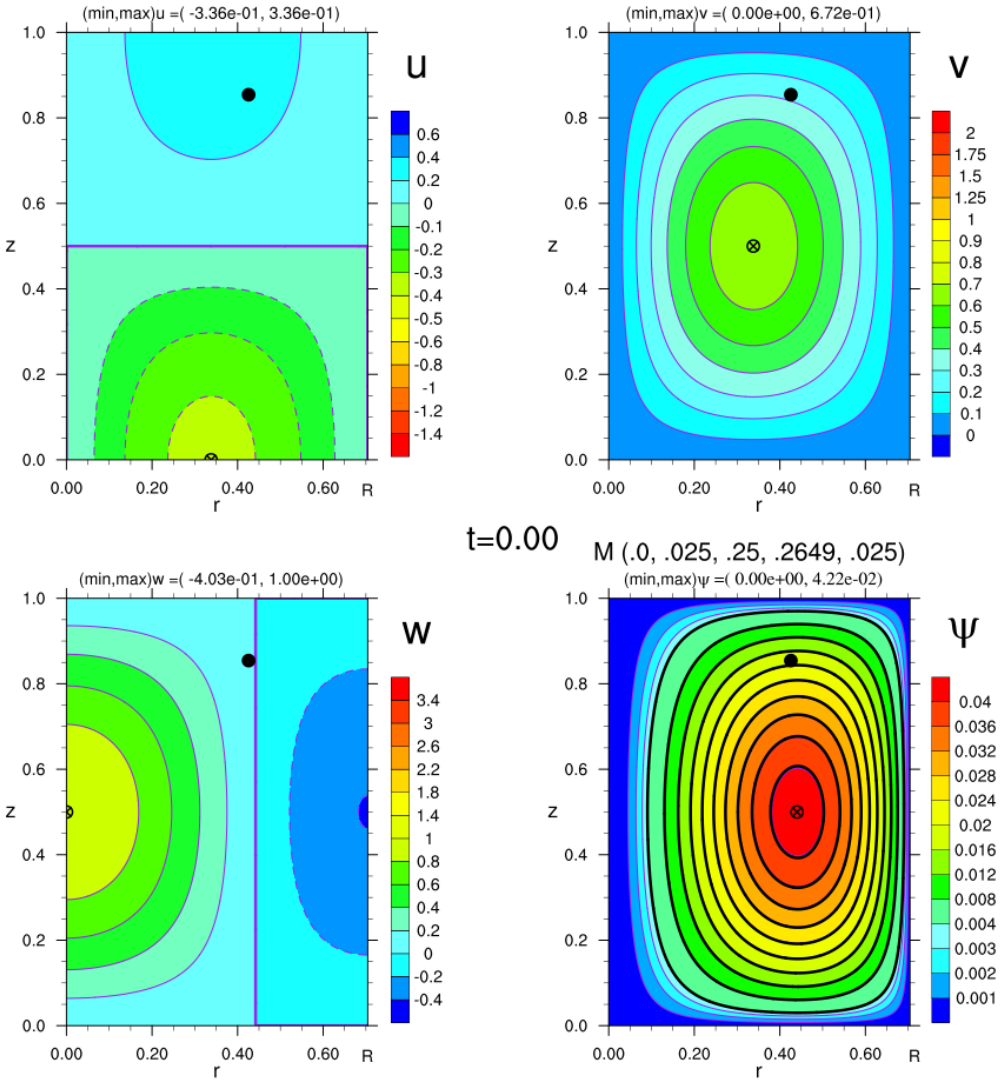

Fig. 2. The velocity components (filled contours), streamfunction (filled contours), and AM (black contours) at t =0. The black dot marks the position of parcel P.

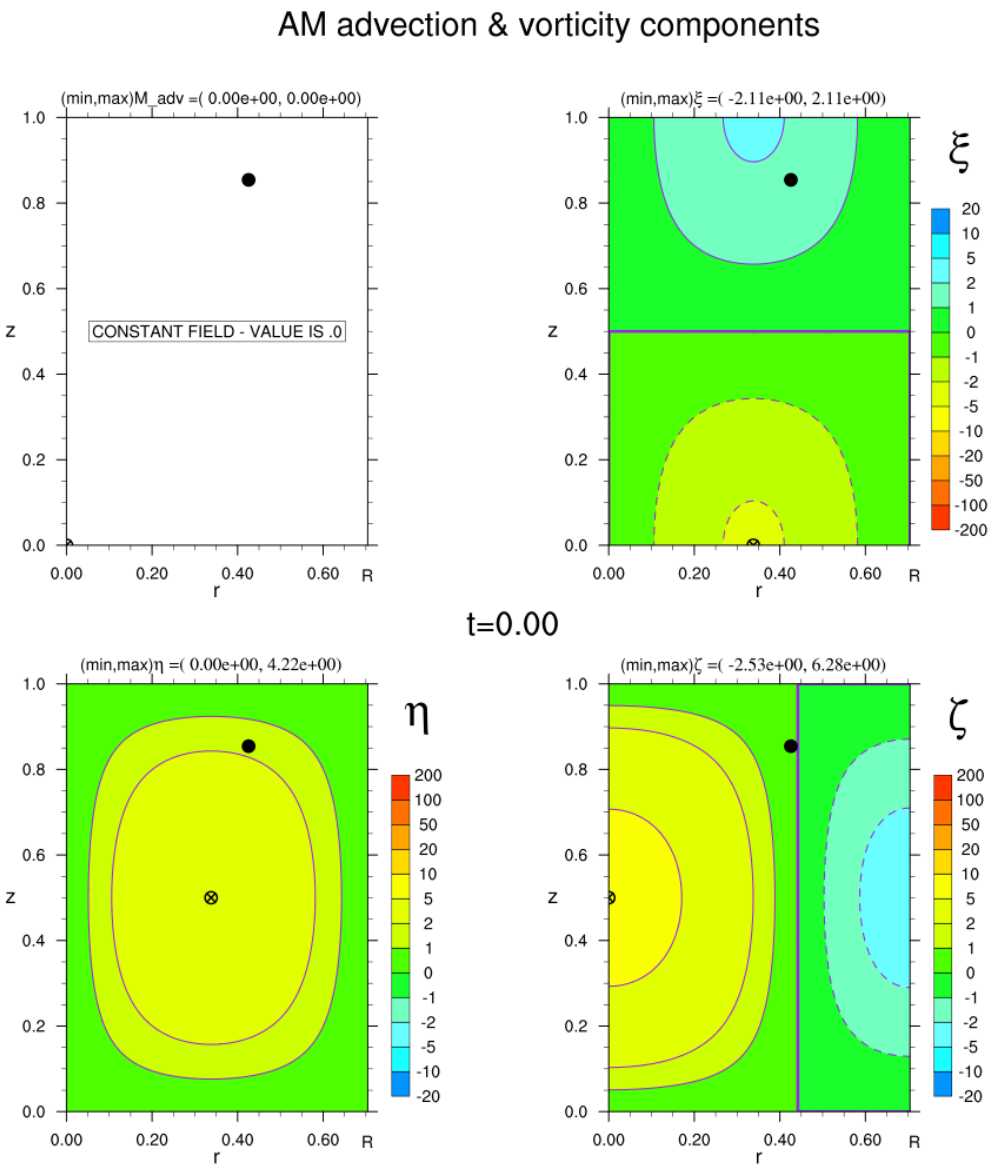

Fig. 3. The vorticity and AM-advection fields at t =0.

I found a parcel P with a forward trajectory that took it into the tornado at t = 5.6. The black dot in the contour plots marks the position of P. Fig. 4 supplies the coordinates of P as functions of time. The parcel moves outward, then down along the outer rim of the domain, at first roughly following a streamline in Fig. 2. It then flows along the surface to near the axis and rises into the tornado at t =5.6. It is at the nadir of its trajectory just prior to t = 5.5 (also evident below in Fig. 7). The nadir is at (r, z) = (0.114, 0.011). Its height above ground is just over 3 grid lengths.

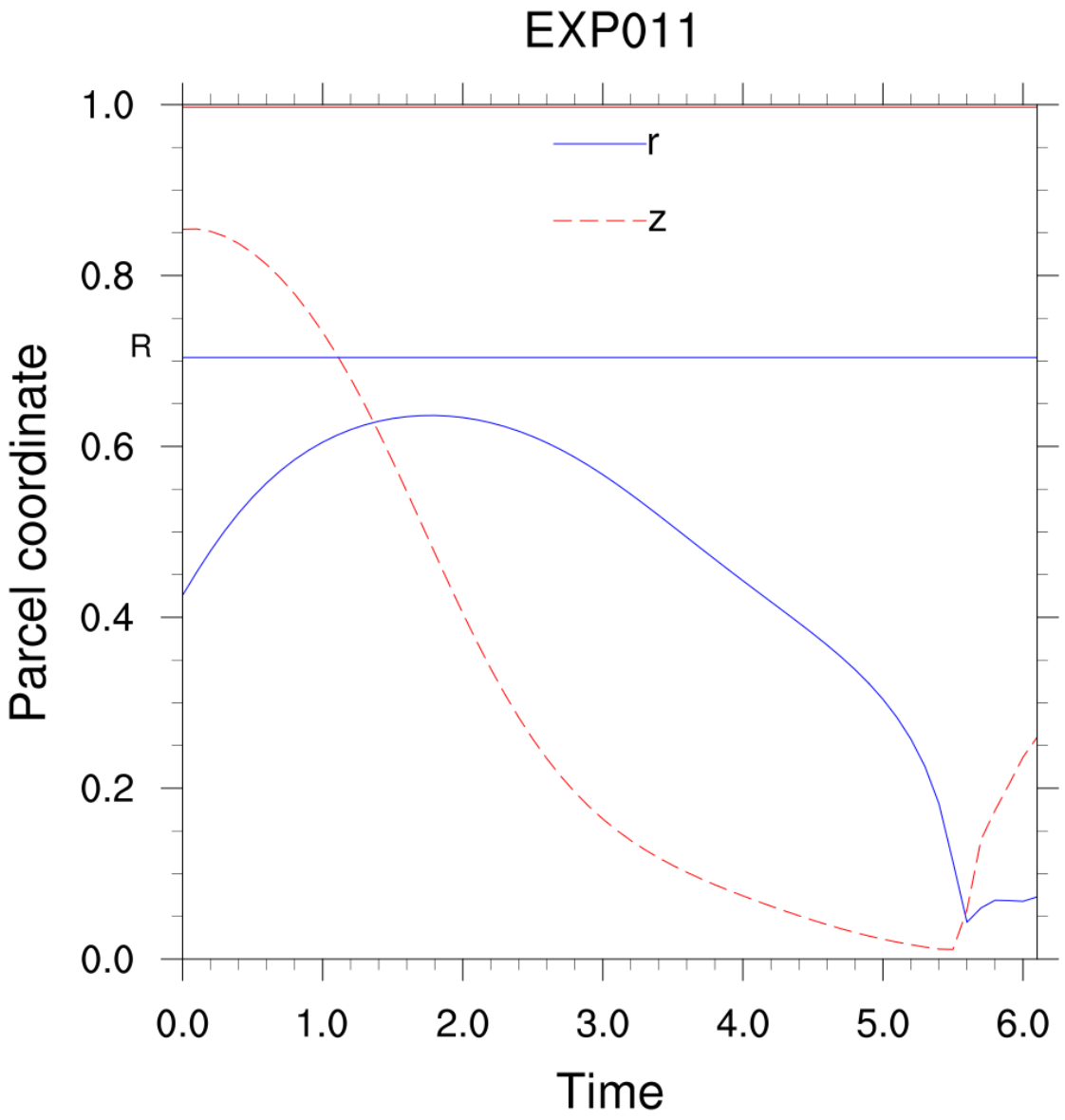

Fig. 4. The (r,z) coordinates of P. The domain top and side are at z = 1 (red line), r = R = .704 (blue line).

At t = 5.4, the time of tornado formation, the parcel is still subsiding, albeit very slowly (Fig. 5). Its vertical vorticity is switching from anticyclonic to cyclonic (Fig. 6). At low heights, the updraft radius is much reduced from its initial size (compare Figs. 5 and 2).

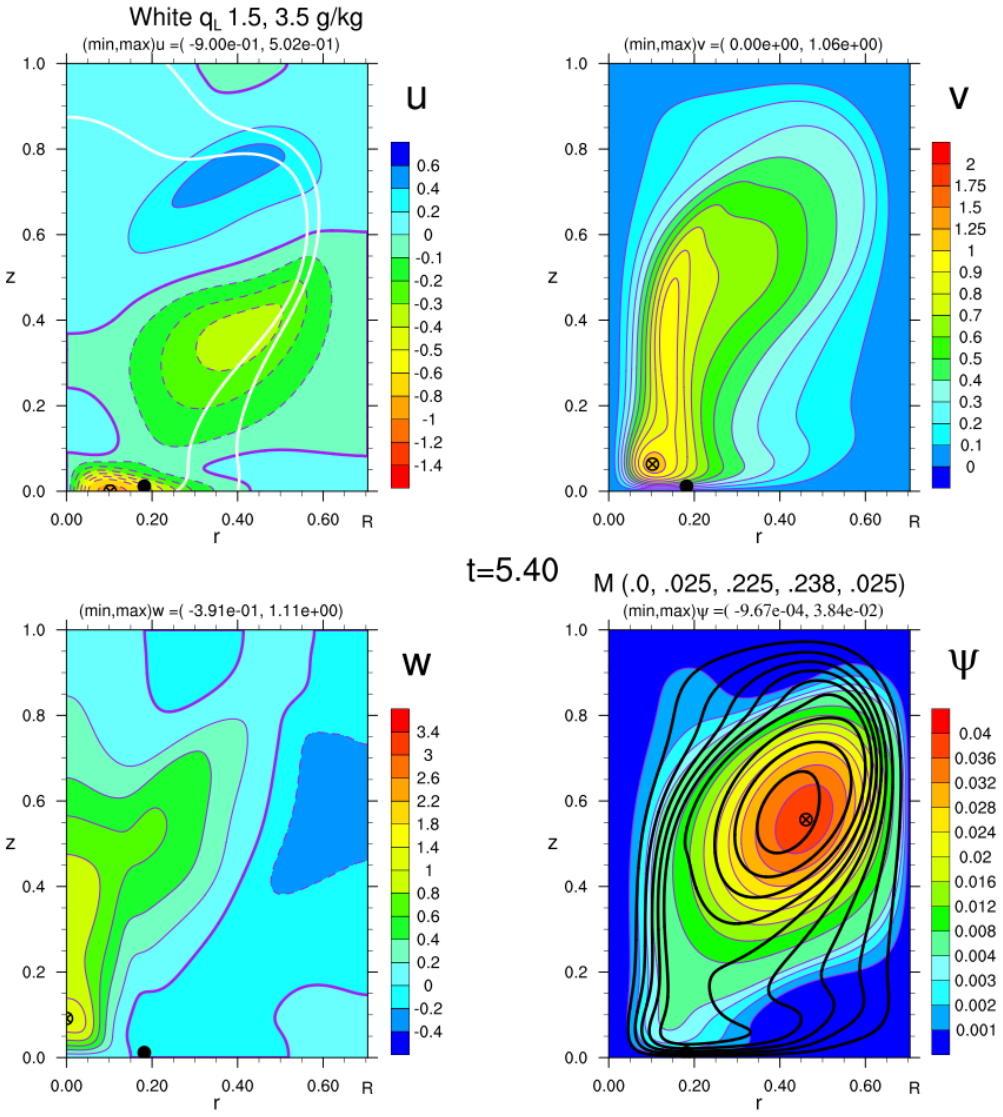

396

397 Fig. 5. As in Fig. 2, but at t = 5.4.

398

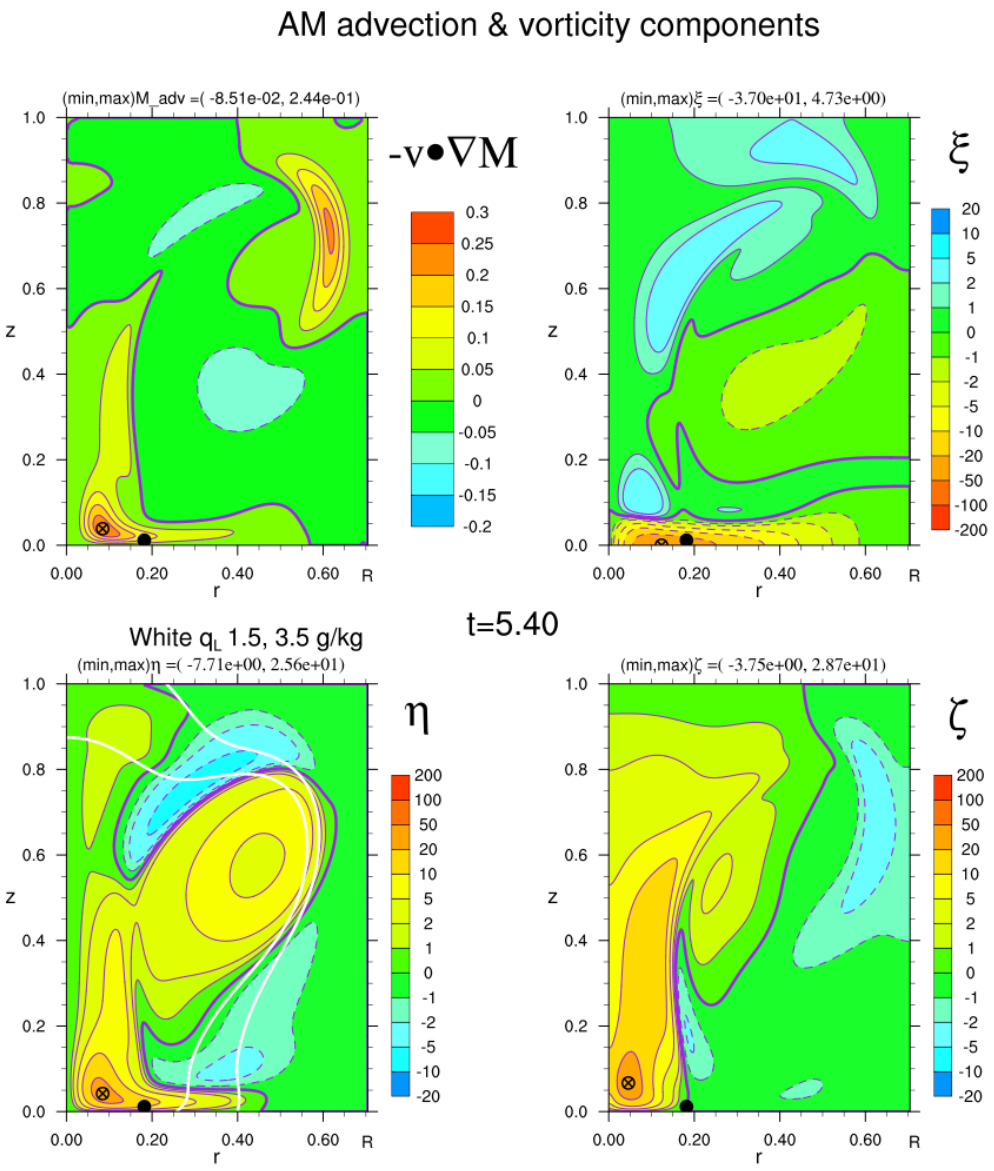

399

400 Fig. 6. As in Fig. 3, but at t = 5.4.

401

402 At t = 5.5, the parcel has just passed its nadir and moved into the updraft (Fig. 7). Its
403 vertical vorticity is cyclonic at the updraft edge so the advection of AM, $r\xi w - r\zeta u$, is positive
404 there (Fig. 8). The no-slip condition on **v** and cyclonic imbalance leads to large inflow and
405 large inward vorticity in the boundary layer of the tornado. Despite the smallness of w and ζ
406 near the ground, AM advection is still significant there owing to the large values of ξ and u.
407 If ζ were zero at the edge of the updraft, AM advection would vanish there, regardless of the
408 magnitudes of ξ and u.

409

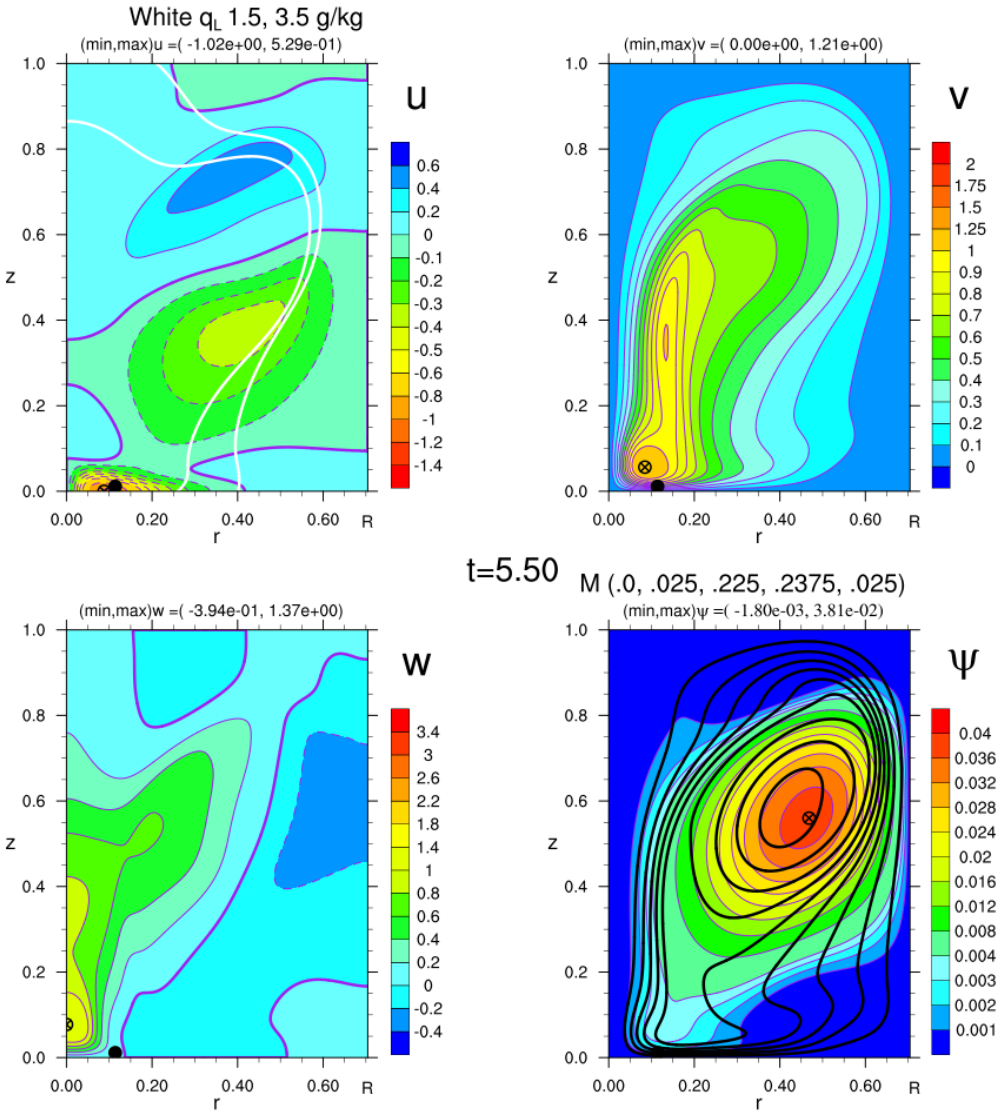

410

411 Fig. 7. As in Fig. 2, but at t = 5.5.

412

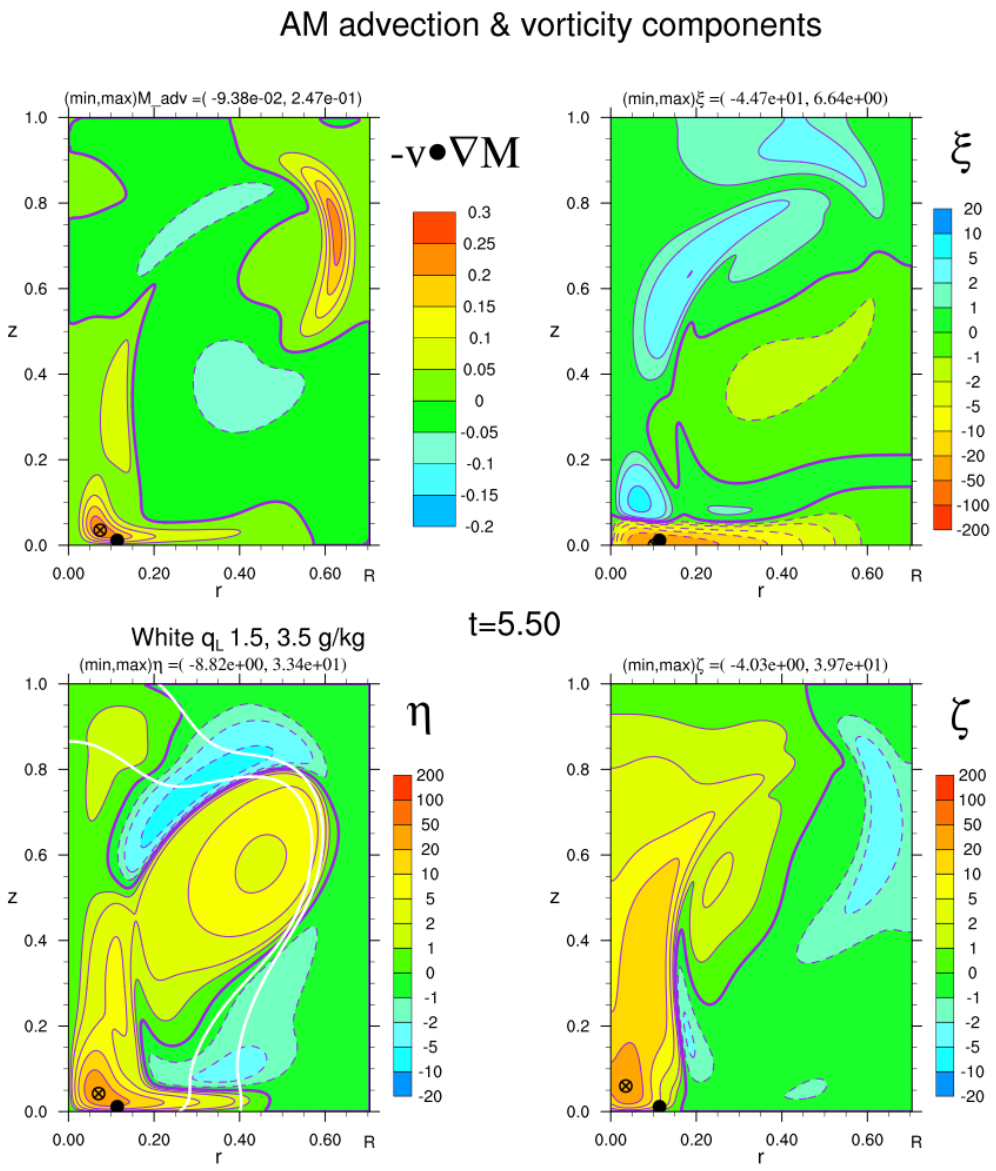

Fig. 8. As in Fig. 3, but at t = 5.5.

Evident in Fig. 8 is the large inward force along the ground owing to the centrifugal force vanishing there. The vertical force is upward near the ground at the updraft edge (Fig. 9). In agreement with (2.14), the air at the edge of the updraft is moving inward faster than the edge. Consequently, the AM advection relative to the inward moving updraft edge is still positive.

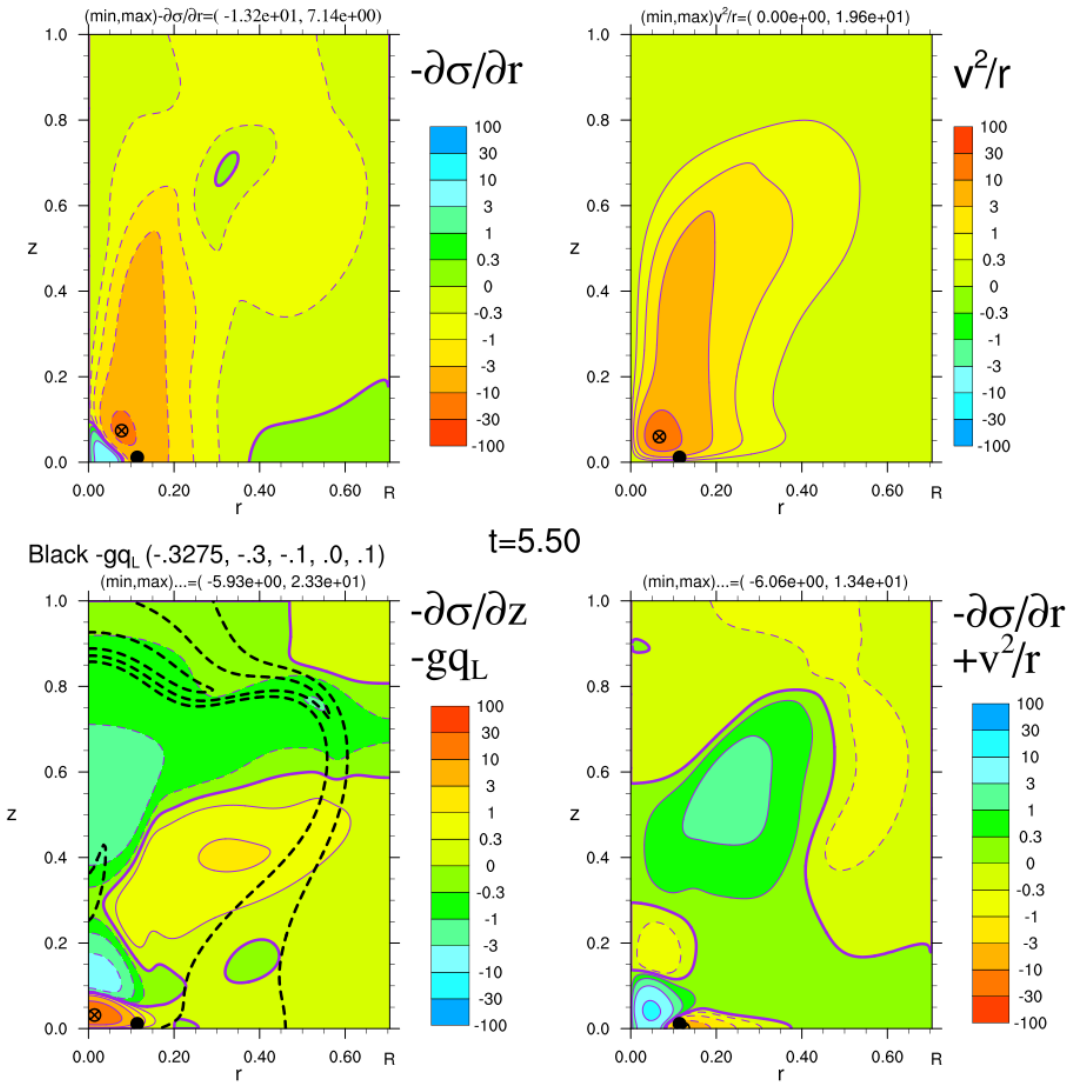

Fig. 9. Forces fields at t = 5.5. The black dot marks the position of parcel P. At this time, it has just passed into the updraft.

At t = 5.6, the tornado has entered the tornado. In contrast to the previous times, its radial vorticity and velocity are now small and its vertical velocity and vorticity are now very large (Figs. 10 and 11).

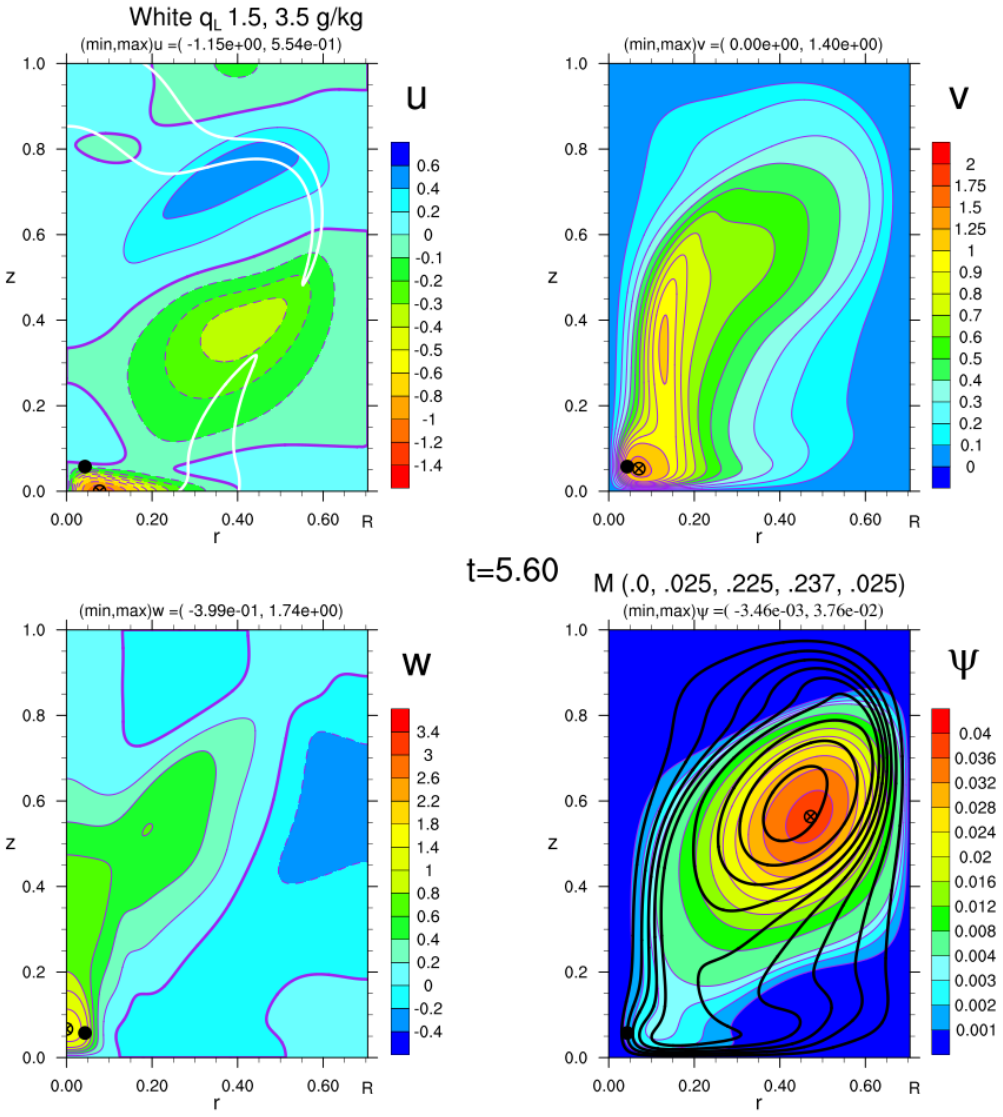

Fig. 10. As in Fig. 2, but at t = 5.6.

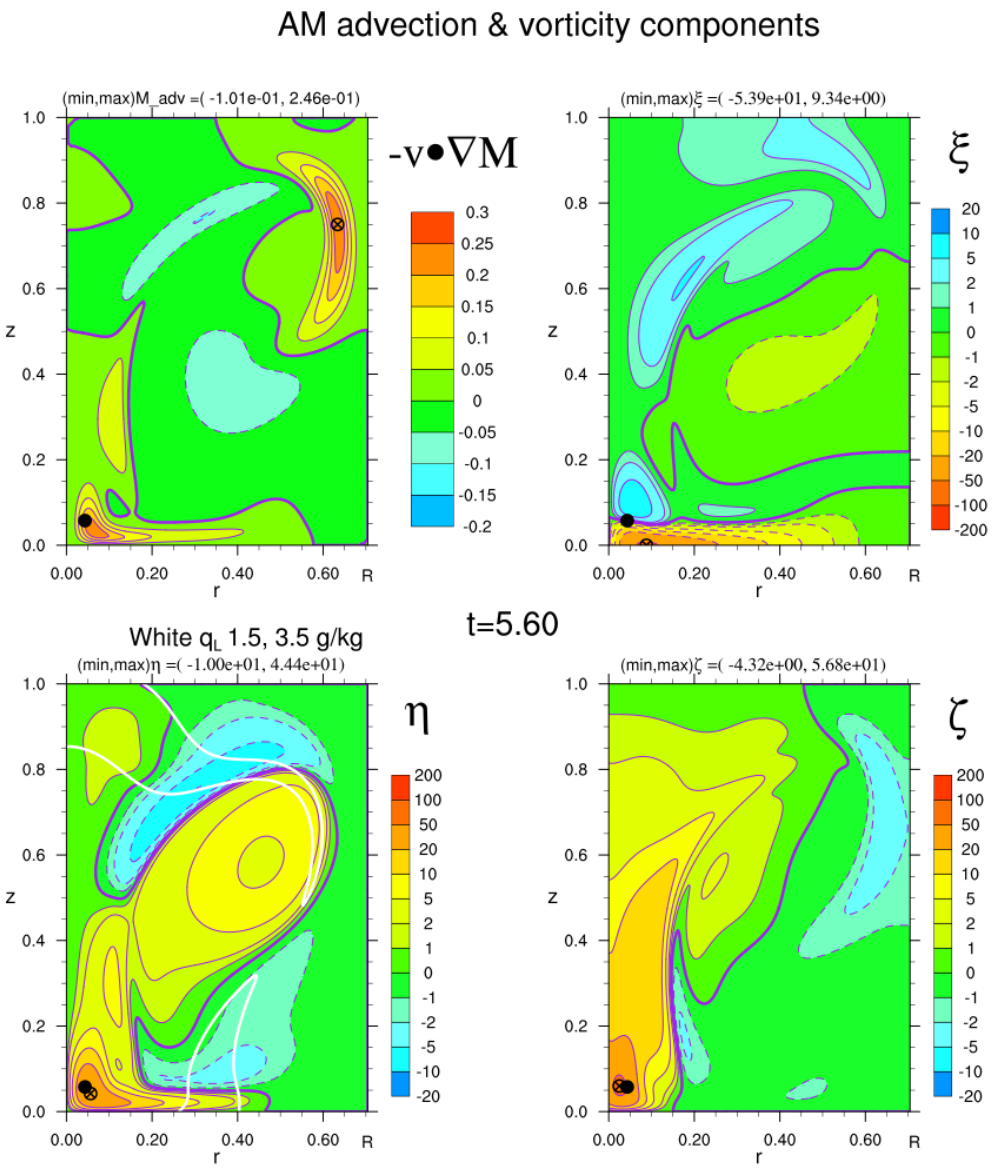

Fig. 11. As in Fig. 3, but at t = 5.6.

The evolutions of parcel P's the velocity components, vorticity components, AM, and AM advection are shown in Figs. 12, 13, 14 and 15. Table 1 lists the values of these quantities when its vertical vorticity vanishes (at t = 5.4), when it is at its nadir (t = 5.47) and when it enters the tornado (t = 5.6). The dimensional height of P is 141 m at t = 5.4, 130 m at the nadir and 692 m at t = 5.6. The parcel's radial velocity (Fig. 12) and radial vorticity (Fig.13) are large and negative at t = 5.4 and 5.5, and practically zero at t = 5.6. The parcel's vertical vorticity (Fig. 13) changes sign at t = 5.4 from negative to positive. From t = 0.1 to t = 5.4, the parcel is in a region of anticyclonic vorticity, never in a patch of cyclonic vorticity.

445 At t = 5.4, its vertical vorticity becomes cyclonic as the parcel is still in its descent. This is
446 due to tilting of large inward vorticity in a weak inward gradient of weak vertical velocity.
447 At the nadir, $\zeta > 0$ as theoretically predicted in section 2. In dimensional terms, the parcel's
448 upward vorticity is a non-negligible $9\text{x}10^{-3}$ s^{-1} at the nadir and it exceeds 10^{-1} s^{-1} in the
449 tornado. Contrary to (2.25), the parcel loses much of its AM as it subsides practically to the
450 ground (Fig. 14). P travels for a long time near the ground in places where the AM advection
451 is positive (Fig. 15). The AM advection increases from t = 1 until the parcel enters the
452 tornado at t = 5.6 and it is high in the time interval 5.4 to 5.6 during the final approach. It
453 then declines as the parcel rises above the level of the vortex breakdown. Table 1 shows that
454 when the parcel's vertical velocity is small, its radial vorticity is very large, and when its
455 vertical vorticity is small, its radial velocity is very large. Since its w and ζ don't vanish at
456 the same place, its AM advection, $r\xi w - r\zeta u$, remains large as it crosses the nadir of its
457 trajectory. This is also evident in Figs. 5-8, 12, 13, 15.

458 For circulation growth around an updraft, the relevant AM advection is curve relative.
459 Since the parcel is moving inward faster that the curve, the curve-relative AM advection is
460 also positive. It is smaller than the absolute one if the updraft is contracting and larger if the
461 updraft is expanding.

462

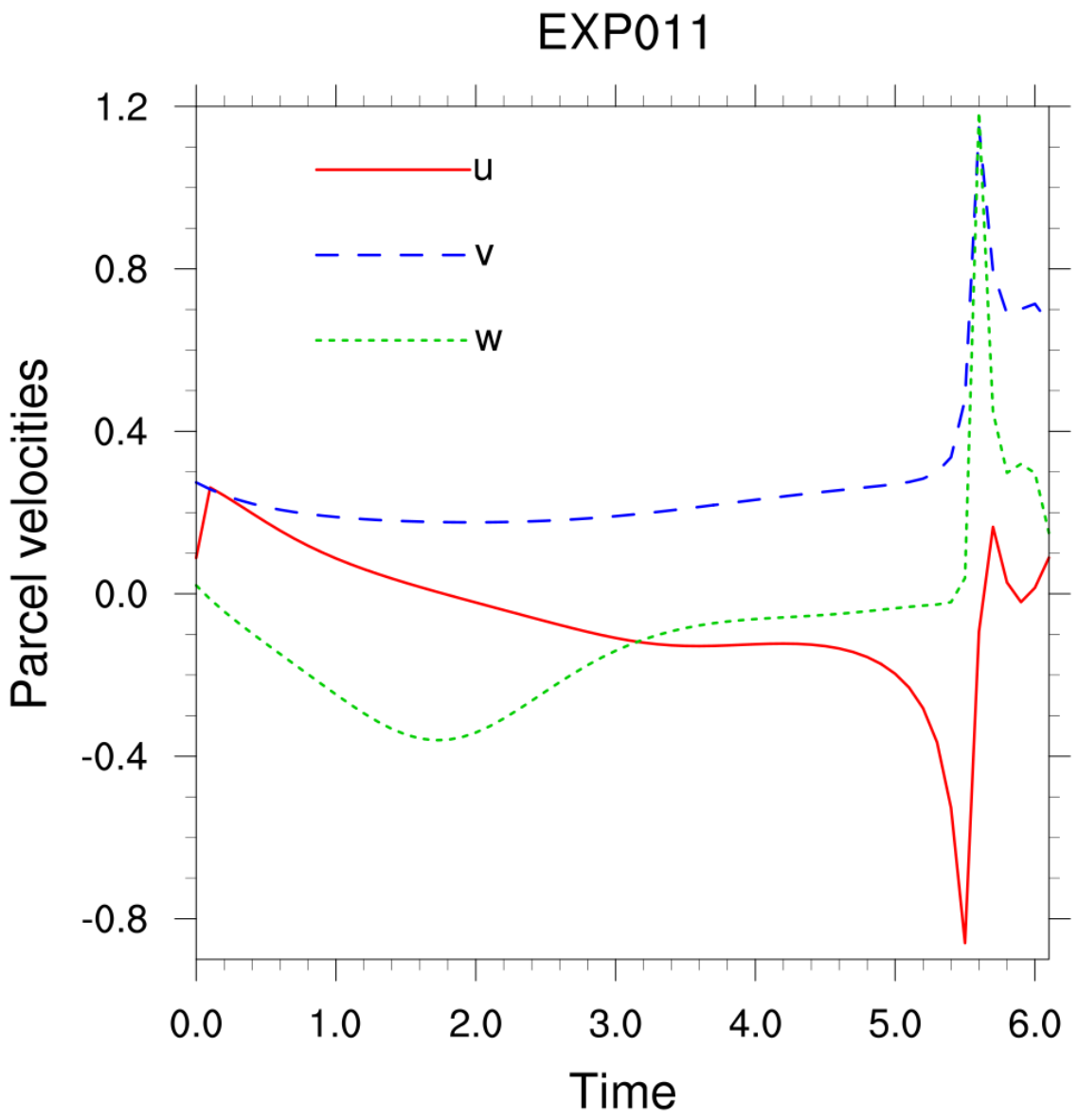

Fig. 12. Parcel P's velocity components versus time.

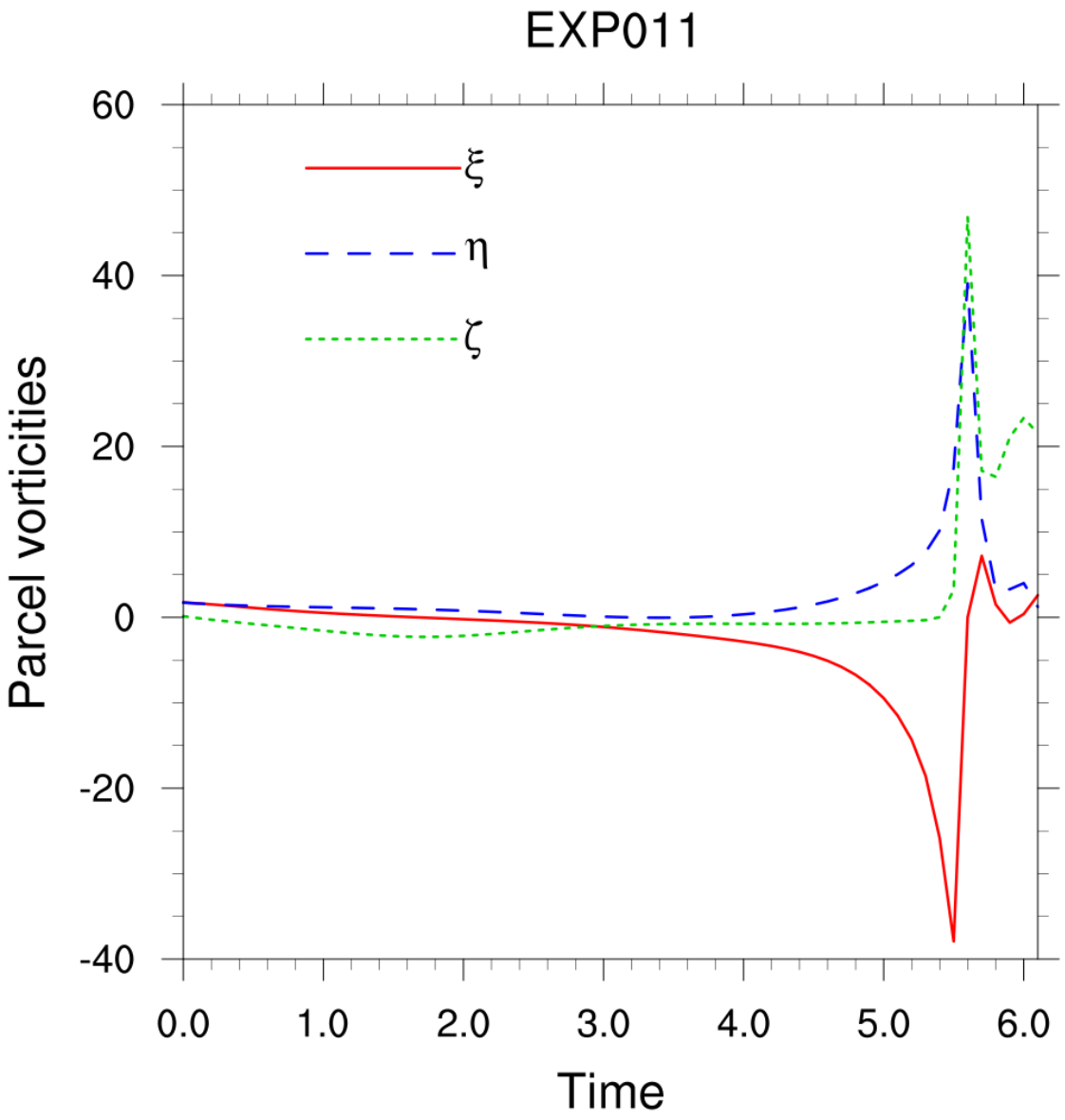

Fig. 13. The parcel's vorticity components versus time.

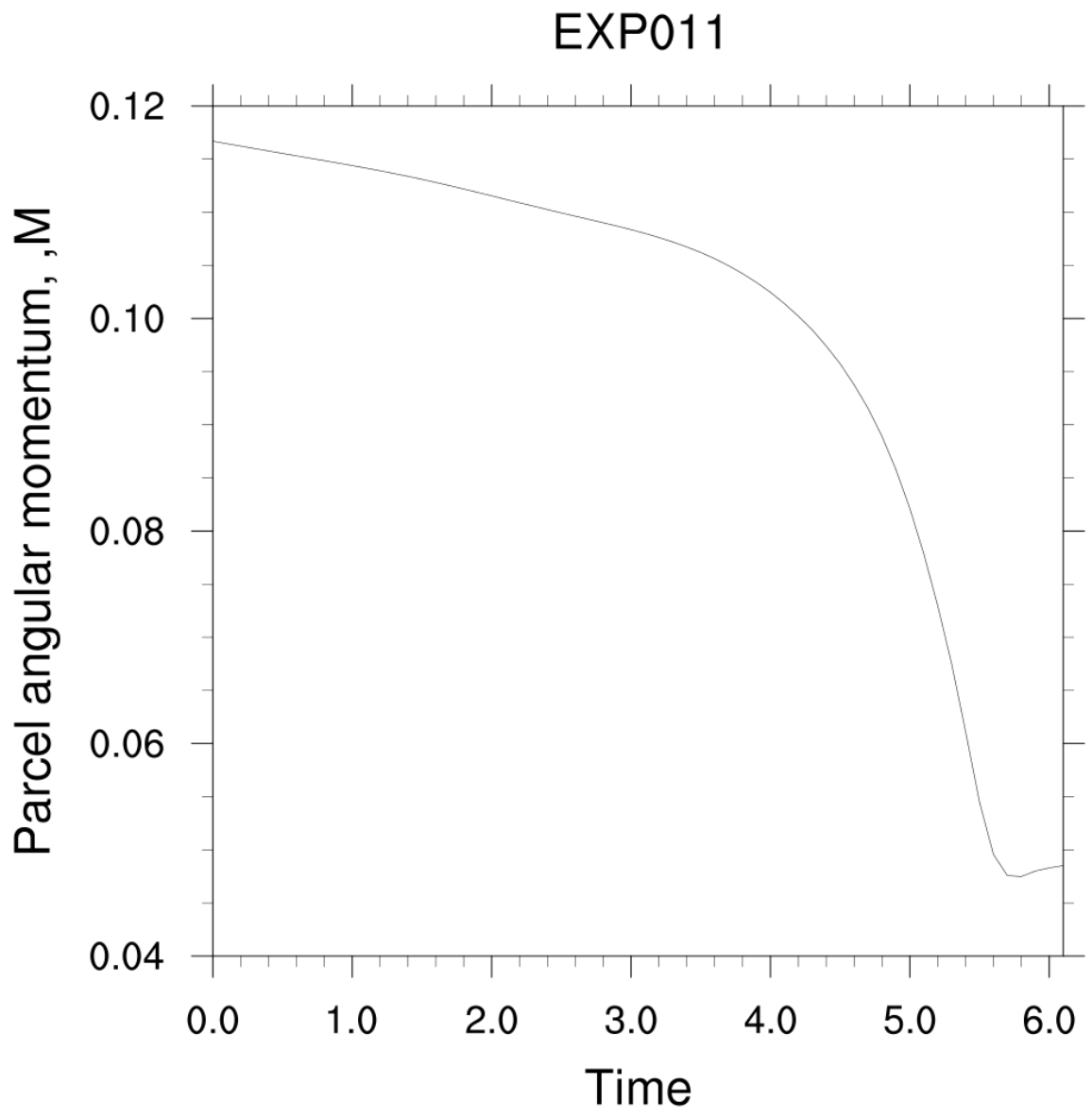

469

470 Fig. 14. The parcel's AM versus time.

471

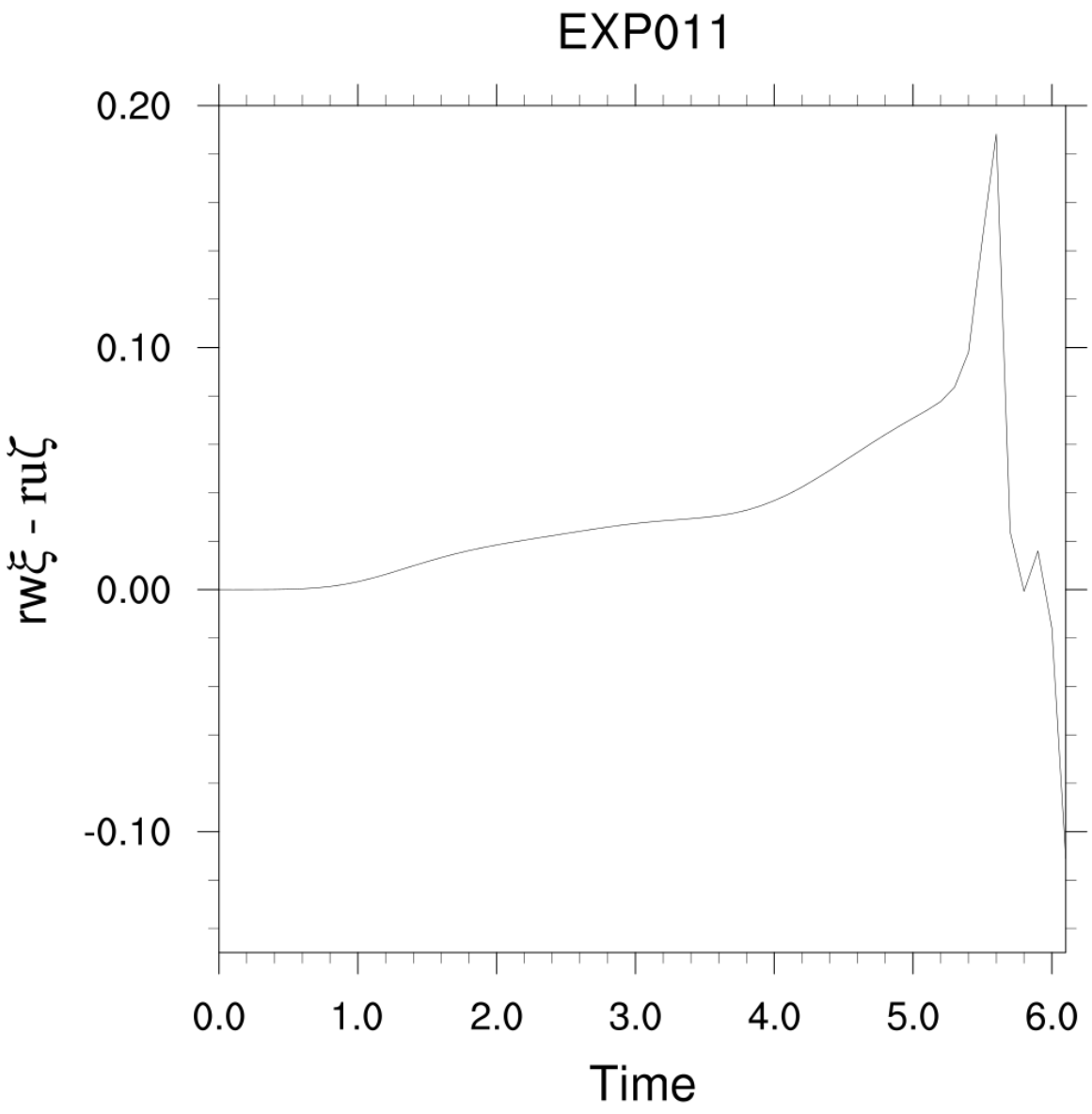

Fig. 15. The parcel's AM advection versus time.

t	(r, z)	u	w	ξ	ζ	$r\xi w - r\zeta u$
5.399	(.182, .0117)	–0.524	–0.021	–25.7	0.002	0.098
5.467	(.140, .0108)	–0.727	0.000	–33.8	1.16	0.122
5.6	(.0432, .0576)	–0.093	1.186	-0.554	46.9	0.190

475 Table 1. Nondimensional values of the parcel's variables near when ζ changes sign (t = 5.398), at its
476 nadir (t = 5.467) and in the tornado (t = 5.467)). The last column is AM advection. Units are 360 s for
477 time, 12,000 m for length, 33.3 m s^{-1} for velocity, and 2.83x10^{-3} s^{-1} for vorticity.
478

479 Following the method of Dahl et al. (2014), we introduced a stencil of parcels to discover
480 how the barotropic vorticity of parcel P as it enters the tornado relates to its vorticity at its
481 nadir. At the nadir, the four stencil parcels are one tenth of a grid spacing above, below,
482 inward, and outward from P. These parcels are tracked from the nadiral time t = 5.467 to a
483 final time t = 5.6 when P enters the tornado (Fig. 16). The barotropic vorticity of P at its
484 nadir and the final positions of the stencil parcels determines the final barotropic vorticity of
485 P according to (2.28). The vorticity of P is independent of intermediate states.

486 First, mass conservation was checked by evaluating the left side of (2.23). We obtain

487 $$\frac{r}{r_i}\begin{vmatrix} \partial r/\partial r_i & \partial r/\partial z_i \\ \partial z/\partial r_i & \partial z/\partial z_i \end{vmatrix} = \frac{0.0432}{0.1402}\begin{vmatrix} 0.0630 & 2.0780 \\ -1.5580 & 0.0124 \end{vmatrix} = 0.998, \qquad (3.1)$$

488 which is close to the exact value of 1. The 'predicted' barotropic vorticity according to (2.28)
489 is

490 $$\begin{bmatrix} \xi \\ \zeta \end{bmatrix} = \begin{bmatrix} \xi_i \partial r/\partial r_i + \zeta_i\, \partial r/\partial z_i \\ \xi_i \partial z/\partial r_i + \zeta_i\, \partial z/\partial z_i \end{bmatrix} = \begin{bmatrix} -2.127 + 2.402 \\ 52.603 + 0.014 \end{bmatrix} = \begin{bmatrix} 0.275 \\ 52.617 \end{bmatrix}. \qquad (3.2)$$

491 where the middle row of Table 1 provides ξ_i and ζ_i and the colors (ξ_i red, ζ_i blue) identify the
492 origin of the terms. The vorticity of P at t = 5.6 in the model is

493 $$\begin{bmatrix} \xi \\ \zeta \end{bmatrix} = \begin{bmatrix} -0.554 \\ 46.880 \end{bmatrix}. \qquad (3.3)$$

494 Although there are discrepancies between (3.2) and (3.3) due to non-barotropic vorticity
495 (generated since P was at its nadir) and numerical errors, it is clear that the vertical vorticity
496 of P in the tornado is due almost entirely to uptilt of its inward vorticity at its nadir, as
497 previously demonstrated by Rotunno et al. (2017).

498 Fig. 16 illustrates how, in the *rz*-plane at least, the vorticity of parcel P is very nearly but
499 not quite streamwise. The associated nonzero Lamb vector is vital. Without it there would
500 not be advection of angular momentum at the downdraft/updraft interface.

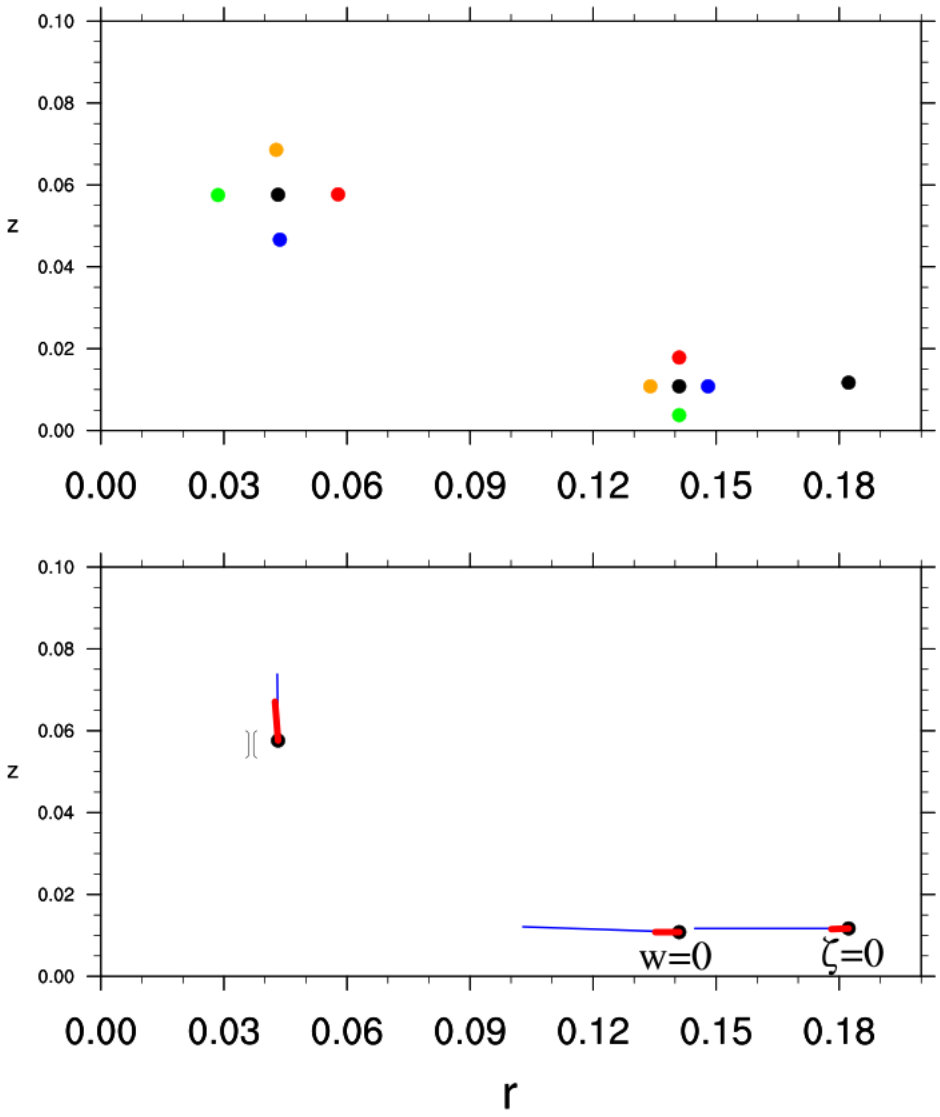

Fig. 16. (Top) Position of parcel P (black dot) when its vertical vorticity vanishes, at its nadir, and when it enters tornado. The stencil of parcels (individually identified by colored dots) is started at the nadir and shown also at the tornado. The spacing of the stencil parcels from P is magnified by twenty for visibility. (Bottom). The velocity vector of P (red) and r times its vorticity vector (blue) when its vertical vorticity vanishes ($\zeta = 0$), at its nadir ($w = 0$), and when it enters the tornado (tornado weather symbol).

Another perspective is gained by examining quantities at the edge of the updraft at a height of 0.0106 (three grid lengths above the ground or 127 m). Between $t = 3$ and 6 the updraft radius at this height contracts to about 25% of its initial size between (Fig.17). Inflow, AM and AM advection at the edge increase immensily as the updraft contracts.

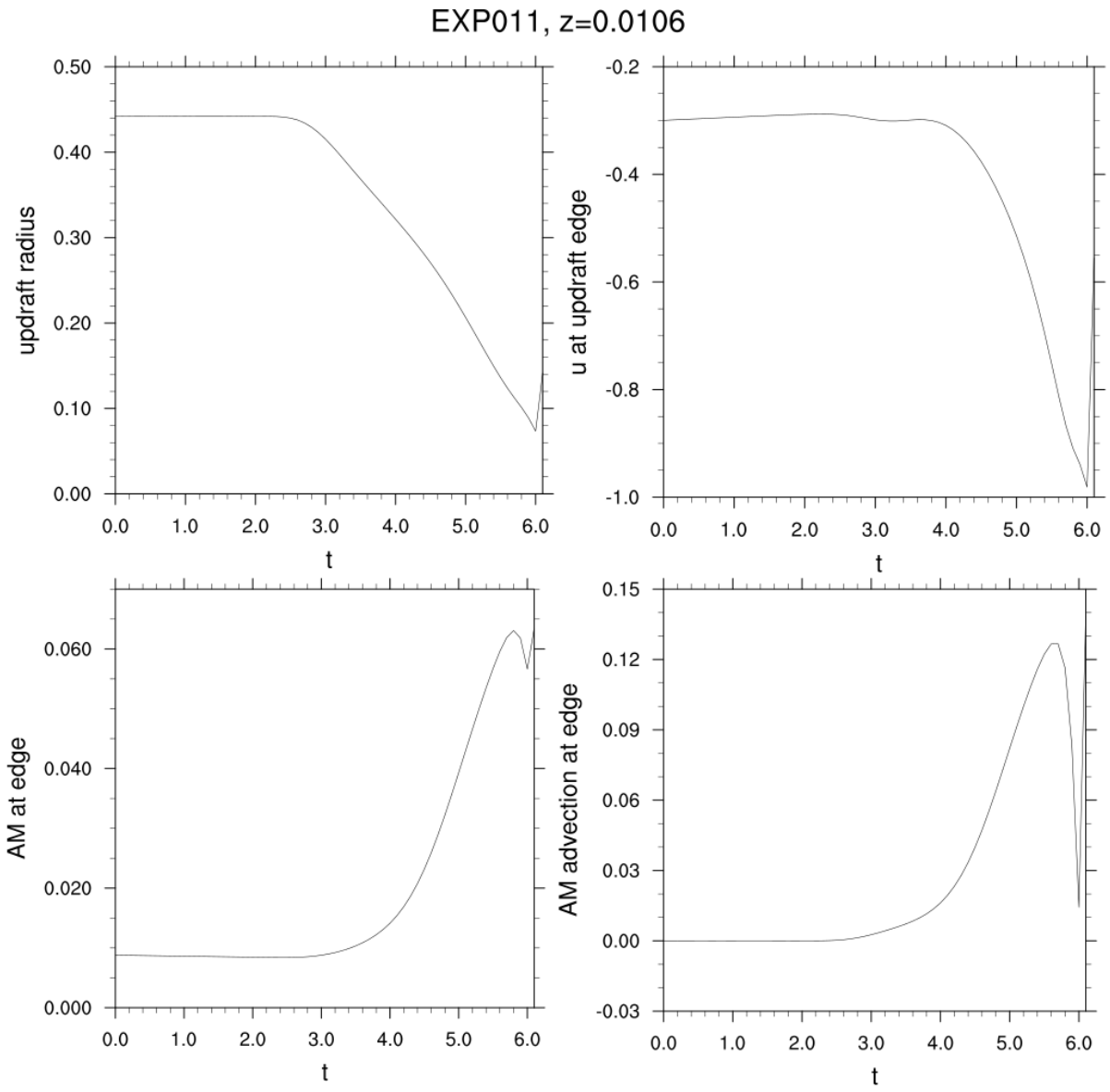

Fig. 17. Evolutions at $z = 0.0106$ of updraft radius and updraft-edge values of radial velocity, AM and AM advection.

The edge values of KE, L and static-energy deficit all become large as the updraft contracts while B declines relatively slowly (Fig. 18).

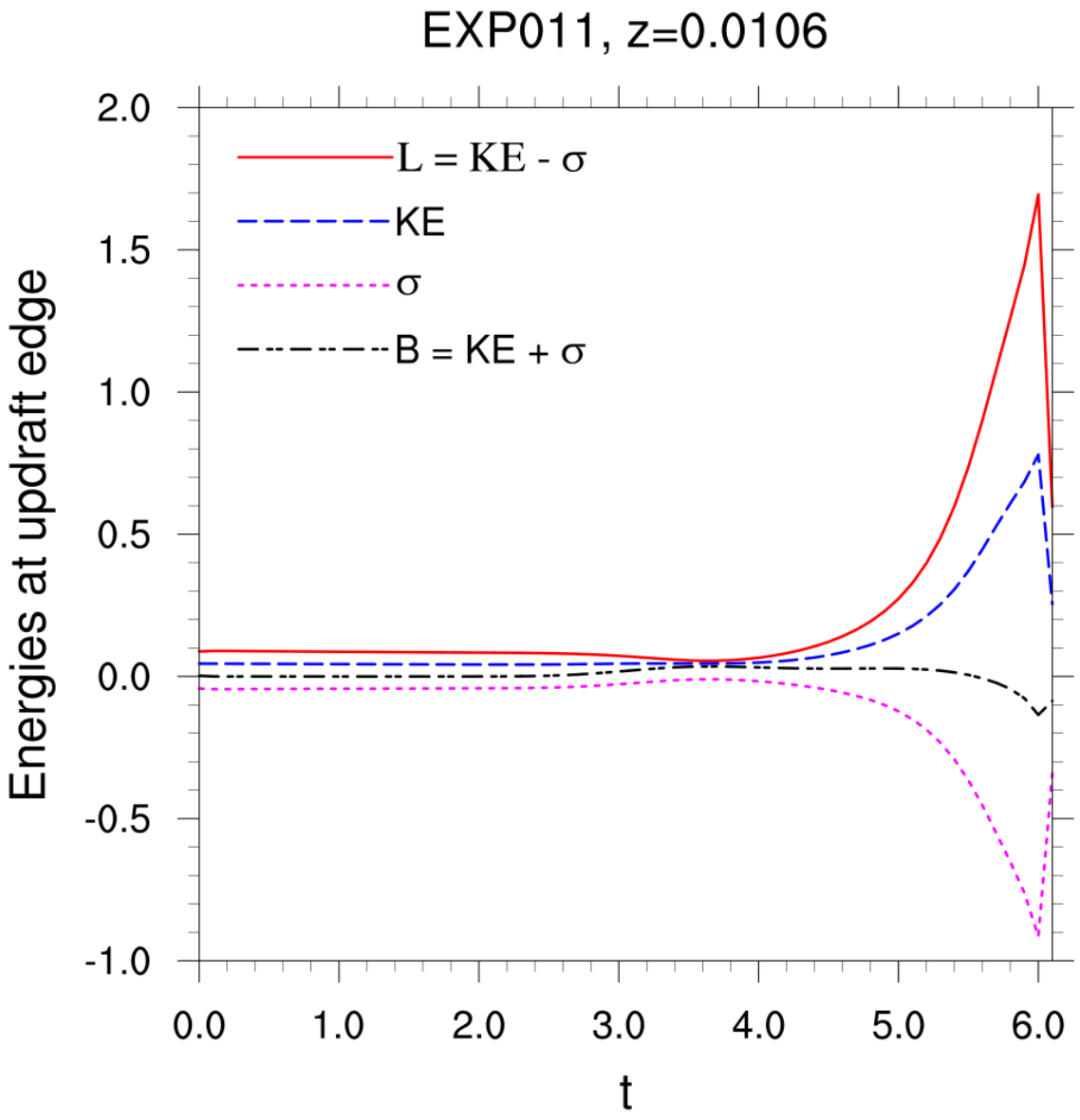

Fig. 18. Updraft-edge values at z = 0.0106 versus time of L, KE, static energy and Bernoulli function.

From their initial values, the near-ground helicity and abnormality at the updraft edge increase by two and one orders of magnitude, respectively (Fig. 19).

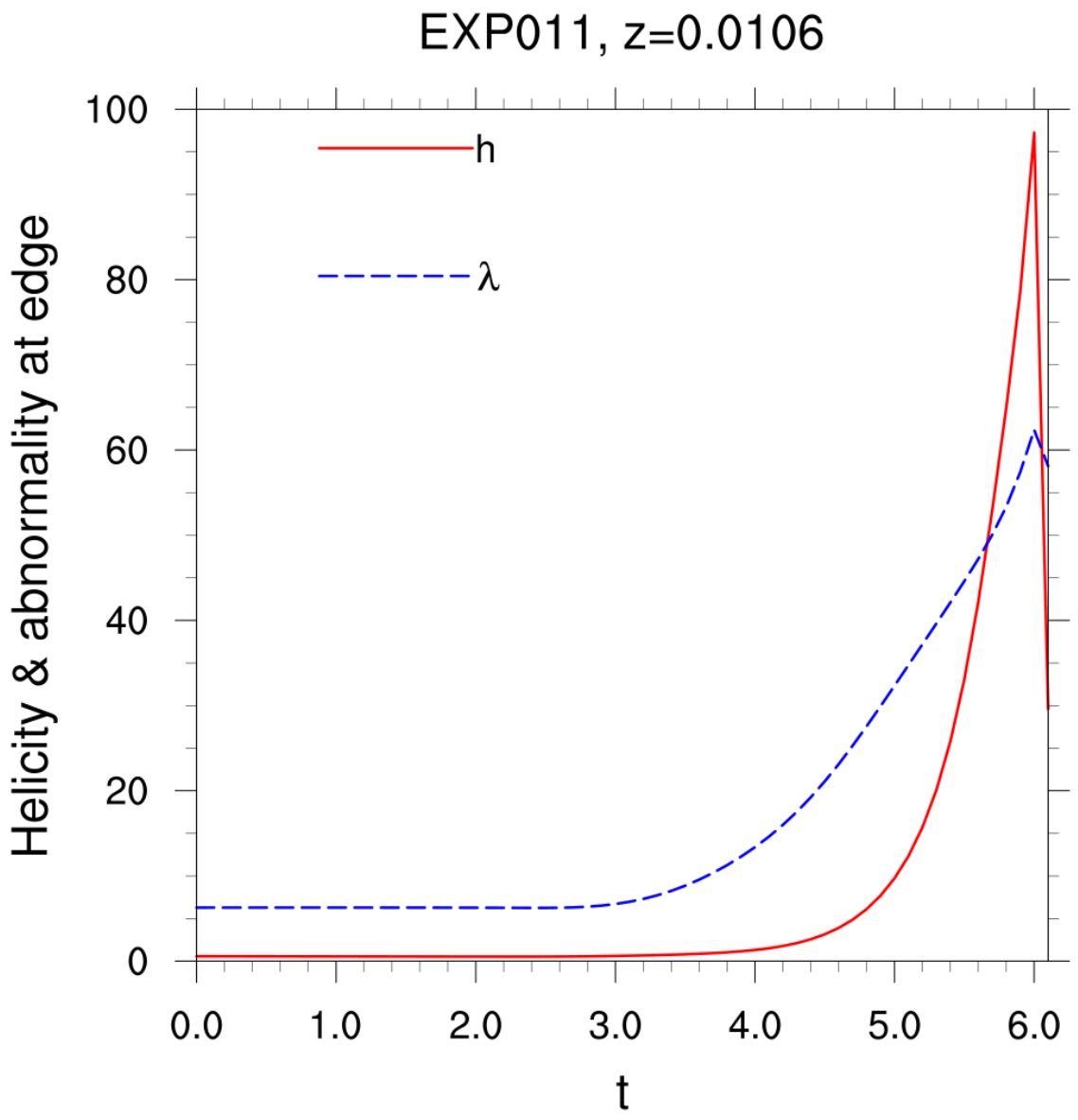

Fig. 19. Growth of helicity and generalized abnormality at height z = 0.0106 on the updraft edge.

The radial vorticity near the ground at the updraft edge is always negative and amplifies greatly during tornado formation and intensification (Fig. 20). In contrast, the vertical vorticity there is much smaller but positive as required for positive AM advection into the updraft.

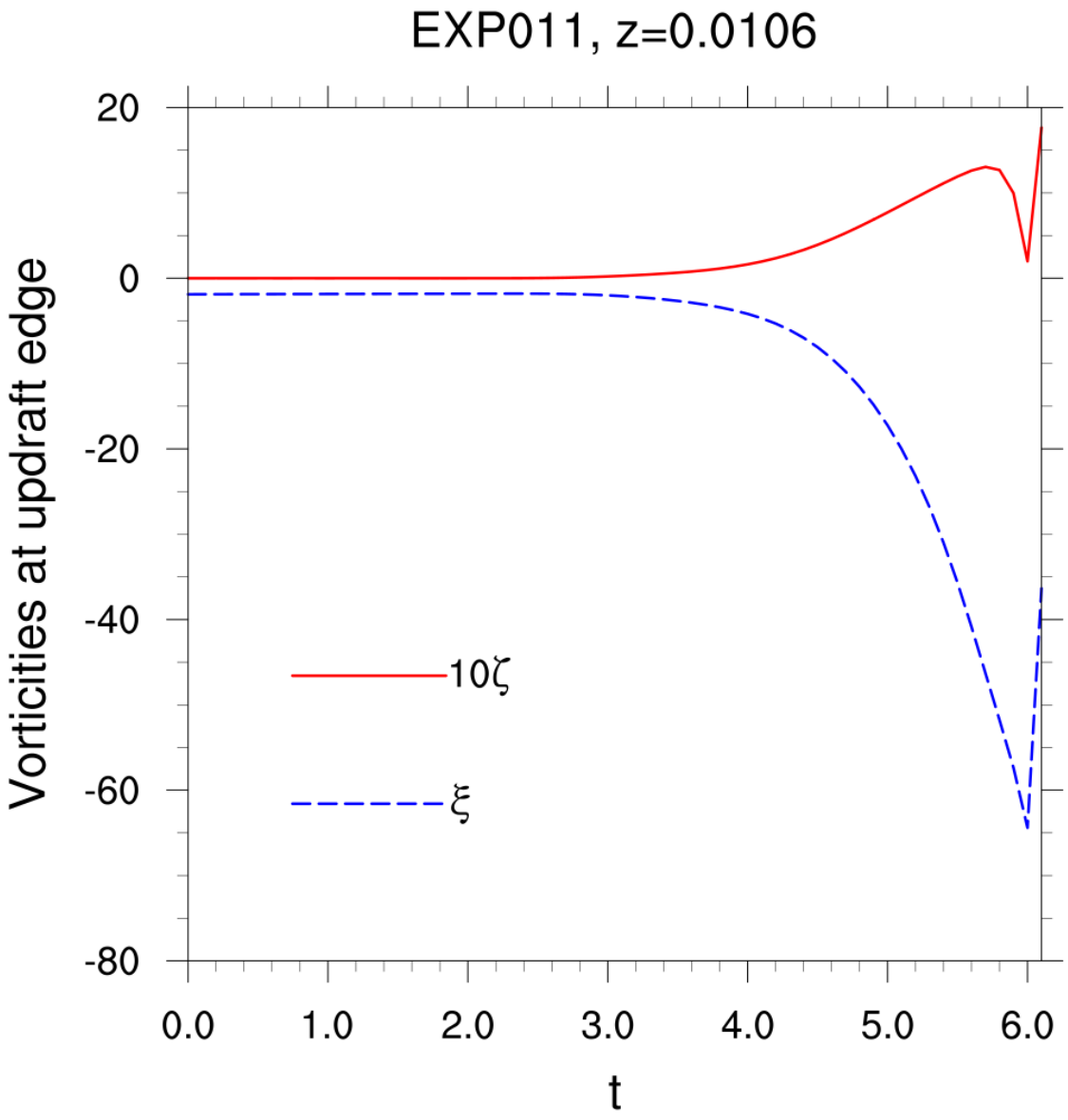

Fig. 20. Edge values versus time of radial vorticity and 10 times vertical vorticity.

4. Summary

Initially in supercells, there is a strongly rotating updraft at mid heights but little rotation about a vertical axis near the ground. How vertical vorticity develops near the ground and materializes as a tornado is a puzzle in tornadogenesis theory. In a Beltrami flow, which has no Lamb vector by definition, there is little rotation near the ground, the circulation around the updraft never increases, and the vertical vorticity always vanishes at the updraft edge.

543 Therefore, the development of low-level updraft rotation must be connected to nonzero Lamb
544 vector and non-Beltrami effects.

545 Headway into solving the above puzzle is achieved herein by concentrating on a level
546 surface at a low height h, defining a closed moving curve such as the edge of an updraft that
547 will eventually produce a tornado, and identifying the processes that cause the circulation
548 around the curve to grow substantially. Eq. (2.9) provides a formula for the rate of change of
549 this circulation. It has barotropic, baroclinic and frictional terms. Increase in the circulation
550 is presumably due to barotropic processes because baroclinic vorticity is primarily horizontal
551 (Dutton 1986, p. 390) and because friction is an important retarding force that typically acts
552 to reduce circulation (Dutton 1986, p. 379) even though it paradoxically aids tornadogenesis
553 (Fiedler and Rotunno 1986). Thus, increasing or even just sustaining the overall circulation
554 generally requires increasing barotropic circulation. According to (2.10), increase in the
555 barotropic circulation around the curve is due to advection of angular momentum at the
556 updraft edge and/or downward turning of inward directed horizontal vorticity at the edge.
557 Eq. (2.12) relates the rate of change of barotropic circulation to the circulation of the curve-
558 relative Lamb vector along the closed curve.

559 If the moving closed curve is the edge of the updraft (the $w = 0$ isopleth), (2.15)
560 demonstrates that cyclonic vorticity and upward force must be correlated at the edge for the
561 barotropic circulation to increase. When the vertical vorticity vanishes at the updraft edge,
562 the updraft's barotropic circulation cannot change and its overall circulation will decay owing
563 to frictional retardation. If, on the other hand, the curve is the $\zeta = 0$ isopleth, then by (2.9),
564 the vertical velocity is downward on the curve when the horizontal vorticity is inward there.
565 Since the vorticity in the supercell environment is predominantly streamwise (Davies-Jones
566 1984), tilting of streamwise vorticity at the start of the downdraft produces anticyclonic
567 vorticity. Hence, the vertical vorticity switches from negative to positive during descent in
568 the downdraft that surrounds the tornado's parent updraft. As air crosses the $w = 0$ isopleth,
569 it carries cyclonic vorticity into the updraft.

570 When the horizontal closed curve is a circle of varying radius, the rate of change of
571 barotropic circulation becomes a line integral around the circle of circle-relative angular
572 momentum [see (2.19)]. If the flow near a tornado is assumed to be axisymmetric, the
573 circulation is simply 2π times the angular momentum (AM) about the center and the integral
574 of (2.19) is (2.20), which states that in axisymmetric flow, the rate of change of AM equals

575 the relative advection of AM at the circle plus the frictional torque there, which near the
576 ground acts to decrease AM. At height h, the mean vertical vorticity of the updraft (its
577 circulation divided by its area) becomes large as the circle contracts and its circulation grows.

578 Thus, a tornado may form only after AM is transported downward to near the ground and
579 inward towards an axis of rotation. At the updraft edge, AM advection is proportional to
580 vertical vorticity so the small cyclonic vorticities that tornado-bound parcels acquire at the
581 nadirs of their trajectories is a sign of AM advection towards the tornado. Without the
582 seemingly insignificant cyclonic vorticity at the updraft edge, the vortex cannot form,
583 intensify and withstand the significant diffusive losses of AM that actually occur in real life.

584 Results from an axisymmetric simulation support these conclusions. In the simulation,
585 the updraft at very low heights contracts so much owing to downdraft intrusion that the edge
586 of the parent updraft is close to the tornado. As found previously (Rotunno et al. 2017). the
587 vertical vorticity that a parcel has in the tornado is due almost entirely to uptilt of the vertical
588 vorticity that it has at its nadir. In the rz-plane, the vorticity of parcels is very nearly
589 streamwise. The nonzero Lamb vector and tiny positivity of vertical vorticity at the nadir of
590 a trajectory are vital however, because without them there would be no AM advection at the
591 edge of the updraft. Formula (2.21) and Table 1 show that this AM advection is the quantity
592 responsible for tornado formation and intensification. It keeps growing during a parcel's
593 final approach to the tornado. This is possible because AM advection is proportional to $w\xi -$
594 $u\zeta$. In the inflow, the radial vorticity ξ is large where the vertical velocity w is small, and the
595 radial velocity u is large where the vertical vorticity ζ is small. The opposites are true in the
596 tornado. The situation where vertical velocity and vertical vorticity are zero at the same time
597 associates with zero AM advection and hence with steady or declining low-level rotation,
598 depending on whether the flow is inviscid or viscous.

599

600 *Acknowledgments.* ____.

601

602 *Data Availability Statement.* Animations of the model results will become available on the
603 author's website.

604

605 REFERENCES

606 Boyer, C. H., and J. M. L. Dahl. 2020: The mechanisms responsible for large near-surface
607 vertical vorticity within simulated supercells and quasi-linear storms. *Mon. Wea. Rev*.,
608 **148**, 4281–4297.

609 Dahl, J. M. L., M. D. Parker, and L. J. Wicker, 2014: Imported and storm-generated near-
610 ground vertical vorticity in a simulated supercell. *J. Atmos. Sci*.., **71**, 3027-3051.

611 Davies-Jones, R. P., 1982: Observational and theoretical aspects of tornadogenesis. *Intense*
612 *Atmospheric Vortices*, L. Bengtsson and J. Lighthill, Eds., Springer-Verlag, 175–189.

613 Davies-Jones, R. P., 1984: Streamwise vorticity: The origin of updraft rotation in supercell
614 storms. *J Atmos. Sci*., **41**, 2991-3006.

615 Davies-Jones, R. P., 2004: Growth of circulation around supercell updrafts. *J Atmos. Sci*., **61**,
616 2863-2876.

617 Davies-Jones, R. P., 2008: Can a descending rain curtain in a supercell instigate
618 tornadogenesis barotropically? *J Atmos. Sci*., **65**, 2469-2497.

619 Davies-Jones, R. P., 2025: Parcel helicity in an axisymmetric model of tornadogenesis. *D-J*
620 *Retirement Papers*, **3**.

621 Davies-Jones, R. P., and H. E. Brooks, 1993: Mesocyclogenesis from a theoretical
622 perspective. *The Tornado: Its Structure, Dynamics, Prediction, and Hazards, Geophys.*
623 *Monogr.*, No. 79, Amer. Geophys. Union, 105–114.

624 Davies-Jones, R. P., and P. M. Markowski, 2021: Circulation around a constrained curve: An
625 alternative analysis tool for diagnosing the origins of tornado rotation in numerical
626 supercell simulations. *J. Atmos. Sci*.,**78**, 2895-2909.

627 Davies-Jones, R. P, R. J. Trapp, and H. B. Bluestein, 2001: Tornadoes and tornadic storms.
628 *Severe Convective Storms*, *Meteor. Monogr.*, No. 50, Amer. Meteor. Soc., 167–222,
629 https://doi.org/10.1175/0065-9401-28.50.167.

630 Dutton, J. A., 1986: The Ceaseless Wind. Dover, 617 pp.

631 Fiedler, B. H., 1994: The thermodynamic speed limit and its violation in axisymmetric
632 numerical simulations of tornado-like vortices. *Atmosphere-Ocean*, **32**, 335-359.

633 Fiedler, B. H., and R. Rotunno, 1986: A theory for the maximum windspeeds in tornado-like
634 vortices. *J. Atmos. Sci.*, **43**, 2328-2340.

635 Fischer, J., and J. M. L. Dahl, 2022: Transition of near-ground vorticity dynamics during
636 tornadogenesis. *J. Atmos. Sci.*, **79**, 467-483.

637 Fischer, J., and coauthors, 2024: Supercell tornadogenesis: Recent progress in our state of
638 understanding. *Bull. Amer. Meteor. Soc*., **105**, E1084-E1097.

639 Lewellen, S., 1993: Tornado vortex theory. *The Tornado: Its Structure, Dynamics,*
640 *Prediction, and Hazards, Geophys. Monogr.*, No. 79, Amer. Geophys. Union, 19–39.

641 Margenau, H., and G. M. Murphy, 1956: *The Mathematics of Physics and Chemistry*. 2nd ed.
642 Van Nostrand, 604 pp.

643 Markowski, P. M., and G. H. Bryan, 2016: LES of laminar flow in the PBL: A potential
644 problem for convective storm simulations. *Mon. Wea. Rev*., **144**. 1841-1850.

645 Markowski, P. M., and Y. P. Richardson, 2014: The influence of environmental low-level
646 shear and cold pools on tornadogenesis: Insights from idealized simulations. *J. Atmos.*
647 *Sci.*, **71**, 243-275

648 Petterssen, S., 1956: *Motion and Motion Systems.* Vol. 1, *Weather Analysis and Forecasting,*
649 2d ed. McGraw-Hill, 428 pp.

650 Rotunno, R., and H. B. Bluestein, 2024: *Rep. Prog. Phys*., **87**, 114801.

651 Rotunno, R., and J. B. Klemp, 1982: The influence of the shear-induced pressure gradient on
652 thunderstorm motion. *Mon. Wea. Rev*., **110**, 136-151.

653 Rotunno, R., P. M. Markowski, and G. H. Bryan, 2017: "Near ground" vertical vorticity in
654 supercell thunderstorm models. *J. Atmos. Sci.*, **74**, 1757-1766.

655 Salmon, R., 1998: *Lectures on Geophysical Fluid Dynamics*. Oxford University Press, 378
656 pp.

657 Shapiro, A., 1993: The use of an exact solution of the Navier–Stokes equations in a validation
658 test of a three-dimensional nonhydrostatic numerical model. *Mon. Wea. Rev*., **121**, 2420–
659 2425.

660 Shtern, V., A. Borissov and F. Hussain, 1997: Vortex sinks with axial flow: Solutions and
661 applications. *Phys. Fluids*, **9**, 2941-2959.

662 Stewart, H. J., 1945: Kinematics and dynamics of fluid flow. *Handbook of Meteorology,*
663 McGraw-Hill, 411–500.